Dynamics of laser-induced cluster Coulomb explosion studied by charge-state and energy resolving ion spectroscopy

Kumulative Dissertation
zur
Erlangung des akademischen Grades
doctor rerum naturalium (Dr. rer. nat.)
der Mathematisch-Naturwissenschaftlichen Fakultät
der Universität Rostock

vorgelegt von
Dzmitry Komar
aus Minsk, Belarus

Rostock
August 2018

Abstract

When a cluster is exposed to intense optical radiation, the particle transforms into a hot expanding plasma. The present work focuses on the ionization, expansion, cooling and relaxation dynamics of laser-induced nanoplasmas. To study the ion emission, we developed a novel charge-state resolving ion energy analyser, which features a high transmission and a high energy resolution. We applied the intensity-difference spectrum method to record the first laser intensity-resolved ion spectra from the Coulomb explosion of clusters and identified two explosion regimes. We deduced the differences in ionization and subsequent recombination between Ar_N and Ag_N. The role of collective excitations on the cluster explosion has been studied by utilizing the pump-probe technique. We obtained ion spectra from metal clusters excited in the impulsive regime. The results show a qualitative difference in the explosion dynamics when compared to studies on rare gas clusters. With respect to long-term relaxation, a significant number of plasma electrons recombines to Rydberg levels of highly charged ions. In experiments conducted on a free-electron laser, a new method to measure the spatio-temporal coherence of XUV radiation has been demonstrated.

Kurzzusammenfassung

Werden Cluster intensiver, optischer Strahlung ausgesetzt, kommt es zur Entstehung eines heißen expandierenden Plasmas. Die vorgelegte Arbeit konzentriert sich auf die Ionisations-, Expansions-, Kühlungs- und Relaxationsdynamik laserinduzierter Nanoplasmen. Um die Ionenemission abzubilden, wurde ein neues Instrument entwickelt, um ladungsaufgelöste Energiespektren aufzunehmen. Vorteile dieses Analysators sind seine hohe Transmission und hervorragende Energieauflösung. In den Experimenten wird die "intensity-difference spectrum" Methode eingesetzt, um erstmals intensitätsaufgelöste Ionenspektren der Coulombexplosion von Clustern zu messen. In der Analyse konnten Unterschiede in der Ionisation und späteren Rekombination zwischen Ar_N und Ag_N aufgelöst werden. Mit Hilfe der Pump-Probe Technik wurde die Rolle kollektiver Anregungen bei der Clusterexplosion untersucht. Weiter ergaben Messungen im sogenannten "impulse regime" einen qualitativen Unterschied in der Explosionsdynamik von Metallclustern im Vergleich zu Arbeiten an Edelgasclustern. In Bezug auf die Langzeitdynamik des Nanoplasmas wurde festgestellt, dass die Plasmaelektronen in Rydbergniveaus hochgeladener Ionen relaxieren. In Experimenten am Freie-Elektronenlaser FLASH wurde eine neue Methode demonstriert, um die räumliche und zeitliche Kohärenz der XUV Strahlung zu charakterisieren.

Contents

List of Figures

Introduction

The detailed description of the interaction between light and matter is one of the fundamental aims of physics. Developments in laser technology have led to the generation of electromagnetic pulses with the electric field strength comparable or even exceeding fields acting on the outermost electrons in atoms [1–4]. This has opened to scientists a new regime of light-matter interaction, i.e., the energy absorbtion depends on the field strength rather than on the photon frequency [5–7]. Strong field excitation of atoms in the gas phase is extensively studied [8–11]. This has led to the development of novel light sources, e.g., emission of light bursts shorter than 50 attoseconds has been reported [12] and table-top sources of bright coherent EUV radiation based on high harmonics generation have been demonstrated [13]. When solids are exposed to strong radiation, collective effects contribute to the dynamics. The number of atoms taking part in the interaction is usually high and uncontrollable. A high fraction of the absorbed energy dissipates into the bulk and only a part of the emitted interaction products can be observed. The disentanglement of effects involved is thus a challenge. Full microscopic numerical calculations to simulate the interaction are currently beyond the capabilities of modern computational science.

To simplify the problem, atomic or molecular clusters can be used as model systems. Clusters represent small particles consisting of up to millions of atoms. They may be produced with controllable size and brought into the gas phase. Since there is no substrate or embedding medium, the laser energy deposited in the system cannot dissipate and the reaction products carry all information about the interaction, in principle. Hence, nanoparticles are ideal targets to study the interaction of strong laser pulses with many-body systems. In the first experiments on clusters in strong fields, many new effects different from atoms have been discovered. When exposed to near infrared radiation, clusters show extremely high energy absorption [14]. This leads to a high ionization degree of cluster constituents [15] and a so-called nanoplasmas formation [16]. MeV ions [17], KeV electrons [18] and X-ray photons [19] are emitted. Even nuclear fusion in deuterium nanoparticles after IR laser irradiation was realized [20]. Since that time, many efforts were made to develop a complete microscopic description of laser-cluster interaction [21,22]. However, the complex dynamics of nanoplasmas remains still a subject of current research. For example, the quantitative description of nanoplasma formation and expansion is not satisfying. The description of recombination dynamics at late stages of the plasma disintegration is incomplete even qualitatively.

The main aim of this work is to provide an extended insight into the interaction of intense laser pulses ($I_{Las} = 10^{13} - 10^{15}$ W/cm^2) with many-body systems such as clusters. Nanoparticles from both conductive materials and insulators are in the focus. We applied ultrashort near-infrared radiation at a wavelength of $\lambda \sim 800$ nm from a Ti:Sapphire laser. Nowadays, most of the high power laser systems operate in the visible or near-infrared, therefore, the understanding of light - matter interaction in this spectral range is of high practical interest, e.g. for laser surface machining [23], high harmonic generation for novel

intense and coherent X-ray light sources [24], ion acceleration for tumour treatment [25], etc.

When clusters are exposed to an intense laser pulse, many phenomena take place which span over very different time scales, e.g., from attosecond electron motion [26] to nanosecond relaxation [27]. In the current work, the ion channel has been chosen to study the evolution of nanoplasmas. Ions preserve the information about charging and acceleration tens and hundreds of femtoseconds after the laser pulse as well as about recombination processes picoseconds later. When ion energies and charge-states are simultaneously resolved, the correlations between phenomena at these time scales may be identified.

In this work, a novel Charge-state Resolving Ion Energy Analyser (CRIEA) has been developed. The new design combines time-of-flight technique with the deflection in a magnetic field, making use of a fast delay line detector. The instrument features a one to two orders of magnitude higher transmission and energy resolution when compared to conventional Thomson parabola spectrometers [28]. High transmission is essential to study metal clusters since they can only be produced in low intensity beams. The instrument has been used to study the long-term nanoplasma relaxation. The understanding of the dynamics at this cluster disintegration stage is essential for the explanation of experimental charge state distributions. Theoretical simulations predict that delocalized electrons, which are trapped with keV energies to a nanoplasma directly after the laser excitation, do not recombine to the ground ion levels during nanoplasma expansion, but stay only weakly bound to ions, e.g., with meV energies [29]. In our experimental studies, a significant amount of highly charged ions were found to carry meV-bound electrons, i.e., highly charged Rydberg ions have been detected. This finding supports the theoretical predictions. Ion emission from clusters was studied in the impulsive excitation regime, i.e., when the laser pulse is short enough to consider the ion core as frozen. We obtained for the first time ion spectra from metal clusters in this regime. The observed emission differs qualitatively from the emission from rare gas clusters [30]. We assume that our studies will motivate further theoretical investigation to find out why the cluster material has a significant influence on the nanoplasma explosion dynamics. The author participated in a large collaborative measurement aiming to record time-dependent parameters such as electron temperature, density, and ionization in laser-induced plasmas conducted on the free-electron laser FLASH in Hamburg. Beside other results, a method to determine the spatio-temporal coherence of XUV radiation, based on a Michelson interferometer, has been realized. This method now can be routinely applied in the free-electron laser beamlines. Additionally, the problem of the signal averaging over the laser intensity distribution in focus has been addressed. In order to attain high laser intensities of 10^{15} W/cm^2, focusing to a spot of about ten micrometer is typical. This circumstance brings up the problem of the laser intensity distribution in the focus. The experimental signal is acquired from the full focal volume and, as a consequence, is averaged over all values of I_{Las}. This has a strong impact on the experimental spectra. In the current work, we apply an intensity-difference spectrum technique [31], which allows us to overcome the effect of focal averaging. First charge state- and intensity-resolved ion energy spectra from argon and silver clusters of different sizes have been obtained. Two cluster explosion regimes have been distinguished. The spectra allow us to deduce the differences in ionization and subsequent recombination between Ar$_N$ and Ag$_N$. Finally, the role of the

collective excitations on the cluster explosion has been studied by utilizing the pump-probe technique. A clear size dependence in the pump-probe studies has been observed.

The manuscript starts with an overview of the current state of research, see Chapter 1. We present features of laser-cluster interaction, basic processes, and typical experimental and theoretical techniques. In Chapter 2, the experimental methods are described with focus on the CRIEA, which is developed in this thesis, and an intensity-difference technique. We overview the results that have been obtained in this thesis in Chapter 3. Finally, we summarize the main achievements of the current work and discuss future perspectives in the outlook. Used methods and results achieved in the thesis are described in detail in the attached publications and appendix.

1. Current state of research

In this chapter, we present an overview of previous studies on the interaction of clusters with strong laser pulses, including basic trends, current theoretical descriptions of the processes as well as well-established experimental methods. We restrict the survey to parameters relevant to the present work. Namely, the interaction of near infrared or visible (wavelength $\lambda_{Las} \approx 400$ nm $- 1\ \mu m$, $h\nu \approx 1.2 - 3.1$ eV) ultrashort (pulse duration $\Delta t \approx 5$–2000 fs) strong (intensity $I_{Las} = 10^{13}$–10^{15} W/cm^2) laser pulses with nanometer clusters of size $\overline{N} \approx 100$–100.000 atoms of different materials is considered.

1.1. Features of laser-cluster interaction

First measurements on clusters in a strong field have shown a drastic difference in their response from that of isolated atoms or small molecules. The typical features of laser-cluster interaction are:

1. **Energy absorption:** A notable property of clusters is their extremely high energy absorption of laser radiation compared to atoms or molecules. At laser intensity of the order of 10^{15} W/cm^2, tens to hundreds of keV may be absorbed per cluster atom on average. Numerous studies on the attenuation of laser pulses in jets of rare gas clusters have been conducted [14, 20, 34, 35]. The measurements show that at laser intensities higher than the barrier suppression ionization threshold*, the cluster gas turns opaque, e.g., absorbing up to 80% of the light, see [14].

2. **Highly charged ions:** The high energy absorption leads to a high degree of ionization of the cluster constituents and subsequent complete cluster disintegration [14]. An example of an experimental charge state distribution is shown in Fig. 1.1, left. The maximum charge state $q_{max}^{Cl} = +20$ significantly exceeds the maximum charge state $q_{max}^{At} = +4$ observed in the case of atomic xenon under the same conditions [36]. To reach Xe^{21+} from an atomic gas, intensities as high as 10^{19} W/cm^2 are necessary [33]. Broad charge state distributions reaching high q are typical for clusters, as have been observed in rare gas [15], metal [37–40], and molecular clusters [41, 42].

3. **Ion recoil energies:** High charging of the clusters leads to their disintegration accompanied by a significant acceleration of the emitted ions, e.g., see Fig. 1.1, right. The energy spectra are usually broad and spread to huge ion kinetic energies. Ions with energies exceeding 1 MeV have been observed from xenon clusters [17], that allows the realization of table-top fusion experiments in dense cluster mater targets [20]. A detailed discussion of ion spectra will be presented below in Sec. 1.5.

4. **Fast electrons:** The recorded electron spectra show that the maximum energy

---

*Description of barrier suppression ionization is presented in section 1.3.1 and in Fig. 1.4
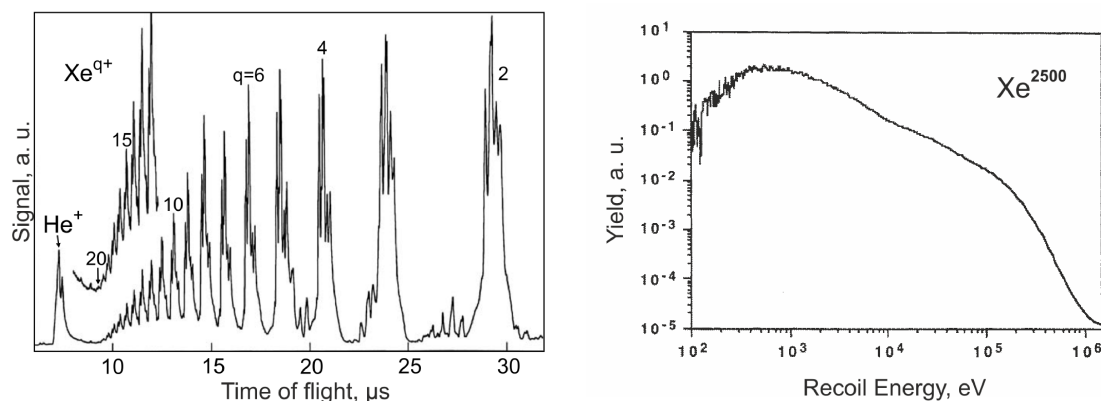
Figure 1.1.: Left: Mass spectrum of highly charged atomic ions from Xe clusters irradiated with 10^{15} W/cm^2, 350 fs, 624 nm laser pulse [32]. The maximum observed charge state $q_{max} = +20$ significantly exceeds the corresponding value observed in atomic Xe under the comparable conditions [33]. Right: Ion kinetic energy distribution from Xe$_{2500}$, exposed to $2 \cdot 10^{16}$ W/cm^2 laser pulses [17].

exceeds typical cut-off energies for atomic targets (i.e., $10\,U_p^*$) by more than one order of magnitude [18, 43, 44]. Electron emission is usually anisotropic with a preferred direction along the laser polarization axis [45–47]. Recently, the control over the electron emission was achieved in SiO$_2$ nanoparticles and metal clusters by applying phase-controlled few-cycle and two-color laser pulses [26, 48].

5. **Soft X-ray emission:** The interaction with a strong laser pulse transforms the cluster into a hot nanoplasma [16]. Electron recombination into core-level vacancies on a timescale up to nanoseconds after the interaction [19, 49, 50] leads to the emission of energetic photons, e.g., photons exceeding ten keV [51]. Numerous studies on X-ray emission from clusters have been performed [52–59] aiming to identify transient charge states in the nanoplasma or to develop new light sources [60, 61].

All of the emission channels are used extensively to reveal the dynamics of the laser-cluster interaction. The aim is to understand the undergoing processes and achieve control by either target preparation or by use of sculpted laser pulses.

1.2. Experimental approaches and challenges

The various information obtained from electron, ion and photon spectra serves as a basis to understand the laser-cluster interaction dynamics. To obtain these spectra, clusters are typically produced as a molecular beam in an ultra-high vacuum chamber. Typically the laser crosses the particle beam at right angle. The reaction products are recorded with corresponding detection systems. In following, we consider each of the experimental parts in detail.

---

*Ponderomotive energy equals the cycle-averaged quiver energy of a free electron in the external electromagnetic wave.
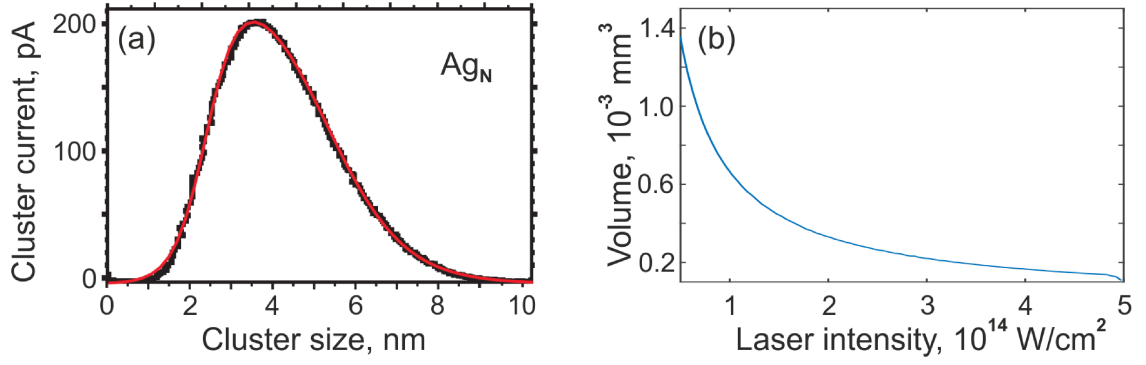
Figure 1.2.: Typical experimental conditions. (a) Size distribution of silver clusters, produced by a magnetron sputterring source. The peak corresponds to $\overline{N} \approx 2000$. The red line represents a log-normal fit to the data. Adapted from [62]. (b) Volumetric laser intensity distribution inside the spectrometer acceptance volume at $I_{Las}^{peak} = 5 \cdot 10^{14}$ W/cm², calculated for the experimental conditions used in Appendix U.

Cluster sources. Signal averaging over the cluster size distribution

Many techniques have been developed to produce clusters in the gas phase [63]. The chosen method depends on material, particle size, and the density of the targets. Clusters from molecules and atoms in the gas phase are mostly obtained in supersonic expansion sources [64–67], which may be constructed in continuous or pulsed versions [68]. To produce particles from conductive solid materials magnetron sputtering sources [69], pulsed arc cluster ion sources (PACIS) [70, 71] and continuous arc cluster ion sources (ACIS) [72,73] are found to be efficient. For conductors as well as isolators, gas aggregation and laser vaporization [74,75] sources may be used. At cryogenic temperatures, He droplet pickup sources have proved their high efficiency [76–78]. Additionally, clusters may be produced chemically and delivered in solvent, which is then sprayed into the vacuum [48]. To get rid of the processing gases or to reduce the cluster gas density, additional pumping stages are often introduced before the particles enter the interaction region.

In general, cluster growth occurs due to collisions of cold atoms in a gas stream. The statistical nature of the process results in a broad distribution of cluster sizes. An example is shown in Fig. 1.2, a. By varying the parameters of the source, the average cluster size may be shifted. However, the width of the distribution is usually of the order of the average size [22]. Therefore, in most of the experiments on the interaction of clusters with strong laser pulses, the recorded signals are averaged over different cluster sizes, thereby obscuring fine structures in the spectra. The resulting influence on the ion signals is discussed in Sec. 1.5. Mass selection is possible, but leads to a significant drop of the target density. In combination with the small volume illuminated by the laser beam, it results in such low count rates that the measurements are infeasible.

Generation of intense laser pulses. Averaging over the focal volume

High power near-infrared pulses are typically generated by laser systems based on chirped pulse amplification [3]. To achieve high intensity I_{Las}, the beam is usually tightly focused

by means of lenses or spherical or parabolic mirrors. Resulting beam diameters typically are of the order of ten micrometers. This allows to reach intensities above 10^{16} W/cm^2 with a table-top laser system. The resulting Rayleigh-limited beam width is usually significantly narrower than the size of the cluster stream and the acceptance volume of the detection system. Therefore, experimental signals are acquired from a volume which includes all intensities from zero up to I_{Las}^{peak}. This effect is called focal averaging. In Fig. 1.2, b, a typical laser intensity distribution in the focus is shown. The volume drops fast with I_{Las}, hence, the signals from the highest intensities are covered with low-I_{Las} signal. The modification of the spectra due to focal averaging is typically strong and has to be considered when analysing the data, see Sec. 1.5. In the current work, we apply an intensity-difference spectrum technique, see Chapter 2, to overcome the effect of focal averaging. This allowed us to obtain first-ever intensity resolved spectra of small argon and silver clusters, e.g., with radius below 100 nm.

For larger particles exposed to X-ray laser excitation, intensity and cluster size selected ion spectra have been demonstrated [79]. In the experiment, the clusters are not size-selected, but the X-ray scattered light is recorded in addition to the ion signal. This signal allows user to assign to each laser shot a size of the cluster in the focus and the applied laser intensity. Later, the obtained spectra are sorted. However, this technique is not applicable for near infrared radiation nor for the particle sizes considered in the current work.

Detection systems

To record the spectra of the particles produced in the interaction, different techniques have been developed. To determine the electron energies, field-free time-of-flight [47, 80] and magnetic bottle spectrometers [81–83] are extensively used. Angular resolved momentum distributions of electrons and ions may be recorded by velocity-map-imaging (VMI) spectrometers [84, 85]. However, VMI instruments usually feature a low energy resolution and only limited energy range. The charge state distributions of emitted ions are recorded by means of mass spectrometry. To measure the ion recoil energy distributions, field-free time-of-flight spectrometers are used. Emitted photons are usually analysed by grating-based spectrometers [86, 87].

Different methods were demonstrated to analyse simultaneously charge states and recoil energies of ions from cluster Coulomb explosions. Among them are retarding field time-of-flight spectrometers [17], magnetic-deflection time-of-flight spectrometers (MD-TOF) [62, 88, 89], and Thomson parabola spectrometers [40, 90–93]. However, the performance of these instruments with low density targets as metal clusters is insufficient. This motivated us to develop a new instrument, described in Chapter 2 and Publication A.

1.3. Laser-cluster interaction dynamics

The interaction of clusters with strong NIR* laser pulse can be represented by a simplified three step model, depicted in Fig. 1.3. In the first step, initial ionization events occur on the

---

*Near-infrared
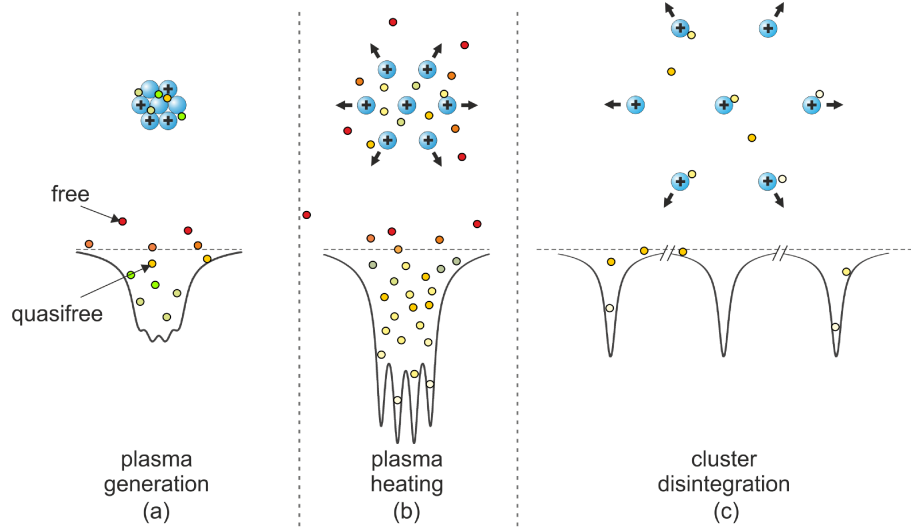
Figure 1.3.: Schematic view of the interaction of the cluster with a strong laser radiation. a,b and c represent three steps of the interaction. See text for explanations.

rising edge of the optical pulse, turning the cluster into a plasma. In the second stage, which lasts as long as the laser field acts on created nanoplasma, cluster constituents are heated and efficient ionization takes place. Finally, the nanoplasma disintegrates into separated ions and electronic deexcitation occurs on a timescale lasting up to nanoseconds. Below we discuss the main processes in more details. We note that due to the large number of particles in the cluster, the theoretical description of the process on the ab-initio level is not possible. Many theoretical approaches have been developed*, and each of them represents a compromise between the computational complexity and accuracy. The quantitative description of the undergoing processes differs depending on the computational model used, so in this survey we overview the processes rather qualitatively. For more details, see reviews [21, 22].

1.3.1. Ionization of atoms in strong fields

The initial ionization of the cluster constituents, which takes place on the leading edge of the laser pulse, is similar in nature to that of isolated atoms in gas. When exposed to laser light, atoms may be ionized even if the photon energy E_{ph} is less than the ionization potential I_p. This happens if the light intensity I_{Las} and thus the photon flux are high enough [94]. The corresponding theoretical analysis was done by Keldysh [95]. He defined that ionization occurs in one of the three regimes depending on I_{Las}, λ_{Las} and I_P, see Fig. 1.4. To distinguish the ionization regimes, the so called Keldysh parameter γ [96] has been introduced:

$$\gamma = \sqrt{\frac{4\pi^2 c^3 \varepsilon_0 m_e}{e^2}} \cdot \sqrt{\frac{I_P}{\lambda_{Las}^2 I_{Las}}} \tag{1.1}$$

---

*The relevant theoretical methods are described in section 1.4
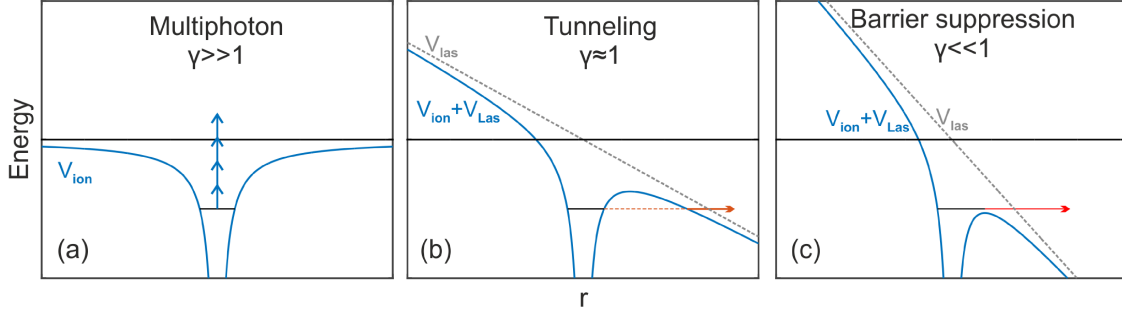
Figure 1.4.: Different ionization regimes of atoms in a strong laser field. (a) In the multiphoton regime ($\gamma \gg 1$, see text), ionization occurs by absorption of several photons. (b) Tunneling ionization ($\gamma \approx 1$) realizes when the laser field bends the Coulomb potential of the atom, allowing the electron to tunnel through the barrier. (c) In the barrier suppression ionization regime ($\gamma \ll 1$), the laser electric field completely suppresses the atomic Coulomb barrier and the electron leaves the atom.

where c is the speed of light, ε_0 is the dielectric constant, m_e is the electron mass, and e is the elementary charge.

In the **multiphoton regime** ($\gamma \gg 1$), the absorption of a number of photons leads to ionization, see Fig. 1.4 (a). The ionization may occur by excitation of atom into virtual levels (non-resonant multiphoton ionization) or to real energy levels (resonant multiphoton ionization). In the latter case, the ionization cross-section is significantly higher. For non-resonant ionization, the rate Γ is then proportional to $(I_{Las})^n$, where n is the necessary photon number.

At higher laser intensities, the field of the pulse starts to play the decisive role. The external electric field may bend the atomic Coulomb potential strongly enough that the electron can tunnel through the formed barrier (**tunneling regime** (TI), $\gamma \approx 1$), see Fig. 1.4 (b). The ionization rate may be calculated applying ADK theory (Ammosov-Delone-Krainov) [97, 98].

Under condition $\gamma \ll 1$, the laser field completely suppresses the atomic Coulomb barrier and releases the electron from the bound level. This regime is called the **barrier suppression ionization regime** (BSI), see Fig. 1.4 (c). The corresponding minimal laser intensity can be calculated as:

$$I_{BSI} = \frac{\pi^2 c \varepsilon_0^3}{2e^6} \cdot \frac{I_p^4}{Z^2} \qquad \text{or} \qquad I_{BSI}[\text{W/cm}^2] = 4 \cdot 10^9 \frac{(I_p[eV])^4}{Z^2} \tag{1.2}$$

where Z is the ion charge state after the ionization. Intensities calculated with Eq. 1.2 correspond well to the ion appearance intensities in atomic gases [99].

For argon and silver, which are the focus of this work, the barrier suppression thresholds are $I_{BSI}^{Ar} = 2.5 \cdot 10^{14}$ and $I_{BSI}^{Ag} = 1.3 \cdot 10^{13}$ W/cm^2. Other relevant material-specific parameters are the ion mass ($m^{Ar} = 39.95$; $m^{Ag} = 107.87$ a.u.), Wigner-Seitz radius ($r_{WS}^{Ar} = 2.21$; $r_{WS}^{Ag} = 1.59\text{Å}$), and I_P. The dependence of I_P on the ion charge state q is shown in Fig. 1.5.
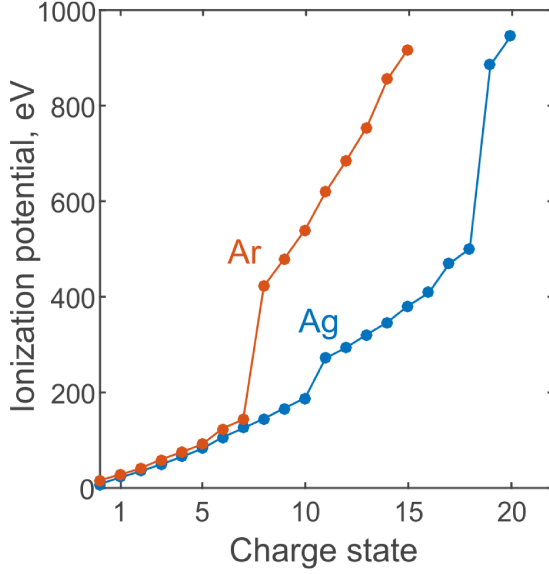
Figure 1.5.: Charge-state dependent I_P of argon (orange) and silver (blue), taken from [100]. In general, I_P^{Ar} is higher then I_P^{Ag}. Pronounced steps at Ar^{8+} and Ag^{18+} may lead to ionization saturation when exposed to intense laser light.

1.3.2. Ionization and heating in nanoplasmas

The mechanisms presented above cannot explain the experimentally observed high degree of ionization in clusters, but they provide a tool to describe the initial ionization, which transforms the target into a nanoplasma. The following dynamics can be comprehensibly treated in terms of inner and outer ionization, as proposed by Last and Jortner [101]. Electrons from first ionization events may leave the cluster, see Fig. 1.3, a. This process is called outer ionization. Due to that, an uncompensated positive charge builds up. The electrons from subsequently ionized atoms cannot quit the cluster and may propagate only within it, see trapped electrons in Fig. 1.3, a. This process is called "inner ionization", and the corresponding electrons "quasifree". It was shown that the presence of quasifree electrons is mandatory for an efficient energy transfer into the cluster [102].

The major heating mechanism in clusters is the energy absorption from the laser field by the scattering of quasifree electrons on the Coulomb potentials of the ions, i.e., by inverse bremsstrahlung. The description of the process depends on the applied theoretical model, see Sec. 1.4. Here we discuss its efficiency and corresponding important parameters only qualitatively. The energy capture depends mostly on the scattering frequency and the local electric field strength and its frequency. Due to the initial bulk ion density, the scattering frequency is high, which leads to an effective energy absorption. However, the electric field strength within the cluster is usually strongly modified by the ions and quasifree electrons, see below. The increase of the kinetic energy of the quasifree electrons leads to additional outer ionization and a corresponding deepening of the cluster mean field potential, allowing even hotter electrons to be trapped, see Fig. 1.3, b. Higher electron temperatures result in enhanced electron impact ionization, i.e., in further growth of the quasifree electron number, which then more effectively absorb laser radiation. This cascade process is often called avalanching [103]. Simulations show that the number of quasifree electrons after the laser pulse is often several times higher when compared to the number of outer ionized [22]. The cloud of trapped electrons responds collectively to the external laser field, significantly changing the electric field strength within the nanoplasma both shielding

or amplifying it depending on the relation of the laser frequency to the Mie-plasmon frequency [63, 104, 105]. The later could be calculated as follows:

$$\omega_{Mie} = \sqrt{\frac{e^2 n_i \langle q \rangle}{3\varepsilon_0 m_e}} \qquad (1.3)$$

where n_i is the density of ions and $\langle q \rangle$ is the average ion charge state.

If $\omega_{Las} \ll \omega_{Mie}$, the electron cloud can effectively screen the laser field inside the cluster, preventing energy absorption. If $\omega_{Las} \gg \omega_{Mie}$, the laser field can penetrate inside the cluster, however, since the energy which electron acquires in the periodic field scales $\propto \omega^{-2}$ [22], inverse bremsstrahlung is not effective. The case when $\omega_{Las} \approx \omega_{Mie}$ is called resonant excitation and leads to the highest energy absorption. Since ω_{Mie} depends on $\langle q \rangle$ and n_i, which are time-dependent, resonant conditions can be realized only transiently [101]. In pump-probe experiments, it was possible to separate the activation process, in which ionization and subsequent expansion are initiated by the first pulse, and the resonant heating, which is realized with the second pulse [106]. The electron cloud, driven in resonance, leads to a significant amplification of the electric field within the cluster, leading to an enhanced electron acceleration, e.g., SPARC-effect* [46], mostly along the laser polarization direction [43–47]. The high intracluster fields reduce the ionization potential of ions, supporting enhanced electron impact ionization [29]. As will be shown in Sec. 3.4 and Appendix U, resonant absorption strongly influences the cluster explosion dynamics, leading to the emission of more energetic higher charged ions.

1.3.3. Ion acceleration mechanisms in clusters

Outer ionization and energy absorption by quasifree electrons result in uncompensated positive charge and high electron temperature in the nanoplasma. Two qualitatively different ion acceleration mechanisms are observed. The first mechanism is realized due to the overall charging of the cluster, i.e., the high potential energy of the ions, which transforms due to charge repulsion into kinetic energy. Cluster expansion driven mostly by that mechanism is called Coulomb explosion. On the other side, if the amount of quasifree electrons is high, their kinetic energy transforms into the kinetic energy of ions during thermalization, accelerating them. That is called hydrodynamic expansion. Both mechanisms contribute to the ion acceleration to some extent. Typically Coulomb explosion is more relevant for the smaller clusters, whereas hydrodynamic expansion dominates for larger particles.

The Coulomb pressure acting on the outermost ion layer is roughly proportional to $1/R^4$, where R is the cluster radius. Assuming a constant electron temperature, the hydrodynamic pressure scales as $\propto R^{-3}$ (see nanoplasma model [16]). Both forces decrease fast with increasing radius; hence, the major part of the ion kinetic energy is typically acquired in the first hundreds of femtoseconds after the laser-cluster interaction. At $I_L = 10^{14} - 10^{15}$ W/cm^2, a considerable cluster expansion occurs already on the order of several tenths of femtosecond. Typically if the pulse length is larger than 50 fs, ion motion

---

*surface-plasmon-assisted rescattering in clusters

has to be considered in the simulations, i.e., cluster charging and expansion take place simultaneously. Ionization and electron heating efficiency depend on the ion density (see Eq. 1.3), whereas ion acceleration, i.e., the change in ion density, is in turn affected by cluster charge and electron temperature. The interplay of these processes make the prediction of final kinetic energy distribution of ions a challenge. In many cases, even finer electron and ion dynamics, e.g., time dependent spatial charge distribution, has to be taken into account. Many studies report the asymmetric ion emission from the nanoparticles predominantly along the laser polarization axis [43, 91, 107, 108]. It is explained by the higher total electric field on the cluster poles, which is a sum of the laser, cluster polarization, and space charge fields. High cluster polarization and space charge fields are established due to the oscillation of the electron cloud and lead to higher ionization degree of atoms at the poles [109, 110] and their stronger acceleration due to the higher field strength [43, 109, 111].

Few-cycle laser pulses allow measurements to be conducted in the impulsive regime, in which the ion motion during the interaction can be neglected [30, 112–114]. In this regime, so-called "unusual" ion emission asymmetry, when ions are predominantly emitted in the direction perpendicular to the laser polarization direction, was reported in rare gas clusters. Several simulations could qualitatively represent this result [115]. The simulations show that the cloud of quasifree electrons in a cluster is stretched along the laser polarization direction, providing effective shielding on the poles and resulting in stronger explosion in the perpendicular direction. However, our measurements on silver clusters, see Sec. 3.2 and Publication C, did not show this effect. The reason of this qualitative difference is still not clear.

1.3.4. Nanoplasma disintegration and relaxation

After the impact of the laser pulse, the nanoplasma expands, hot quasifree electrons cool down and partially recombine, see Fig. 1.3, f. In this stage, the final ion charge state distribution (CSD) is formed. Understanding of the underlying processes is necessary to explain the experimental observables. However, a simulation of the long-term dynamics is time-consuming, since nanoplasma cooling and electron localization may last tens of picoseconds [29]. The lifetimes of electron excitations in ions extend up to nanoseconds after the laser pulse [27, 116]. Outer ionization is still going on during cluster expansion due to the energy exchange between electrons and subsequent thermal evaporation. The recombination of the cold electrons provides an additional electron temperature increase mechanism in exploding cluster [79].

Molecular dynamics simulations have shown that, at specific conditions, most of the quasifree electrons that were initially strongly bound to the nanoplasma, may never recombine or recombine to only high-lying Rydberg states of ions during the nanoplasma expansion [29]. This effect is called frustrated recombination. To qualitatively understand the process, three-body recombination, which is treated as the main recombination mechanism within a plasma, has to be considered. The rate $\mathcal{R}$ is typically expressed as $\mathcal{R} \propto n_i n_e^2 T_e^{-4.5}$, where n_i and n_e are the ion and electron densities and T_e is the electron temperature [117]. Early in the cluster expansion, the quasifree electrons are hot and the recombination rate is low. Later, the cluster expands and the electrons cool down adiabat-

ically. The particle densities n_i and n_e are then low, preventing efficient recombination. However, the mean field potential flattens during expansion, and the electrons net energy approaches zero. The presence of weakly bound electrons in a nanoplasma was proven experimentally [118, 119]. Weakly bound electrons may easily be removed by the spectrometer extraction or space charge fields, which modify the final charge state distribution. An energy exchange mechanism between the Rydberg electrons in nanoplasma, called correlated electronic decay, was observed, leading to emission of electrons with energy close to the ionization potential [119]. Autoionization during cluster disintegration was also obtained experimentally [120]. Within this thesis, an experimental study of the emission of highly charged ions carrying Rydberg electrons from cluster Coulomb explosion has been conducted. The results are presented in Sec. 3.1 and Publication B.

Additional effects take place if the density of the cluster gas is high, e.g., $\rho_C \approx 10^{14}$ cm^{-3}. The sheath of Rydberg excited clusters is formed around the laser focus, thereby efficiently neutralizes ions emitted from the focus [121, 122]. Charge capture and even formation of negative ions is then possible [123].

1.4. Theoretical approaches

Due to the large number of particles, simplifications have to be made to make the calculation feasible. An overview of the theoretical methods can be found in [21, 22]. Here we briefly describe mostly used and relevant approaches with respect to this thesis.

Since the amount of energy deposited per particle at the considered laser intensities is known to be huge, a classical treatment is a good approximation. One of the earliest and simplest ansatzes is the nanoplasma model, originally formulated by Ditmire et al. [16]. Briefly after the initial ionization, the cluster is treated as a spherical nanoplasma of radius $R(t)$. The model parameters such as electron and ion density as well as electron temperature are assumed to be uniform within the cluster. This approximation was later relaxed by including R-dependent parameter distributions [124]. The heating rate is calculated by considering the laser energy deposition rate in a dielectric sphere. Ionization is treated by rate equations as well, which include empirical coefficients. Cluster expansion is determined by the sum of the Coulomb and hydrodynamic pressures acting on the cluster border. This oversimplified model includes the main processes taking place in the cluster. However, a couple of effects are neglected, e.g., attenuation of the laser field by the absorption in the cluster, any effects taking place due to inhomogeneities in the plasma, etc. With the nanoplasma model, only averaged and often inaccurate values of the parameters may be calculated. However, the advantages of this method are easy implementation and low computational requirements, suitable for a conventional personal computer.

A more complex model is molecular dynamics (MD) simulation. Many groups developed MD codes to simulate laser-cluster interaction [29, 125–135]. Particles are treated individually and their motion is described by solving the classical equations of motion. Field ionization is usually calculated by ADK [97]. Semi-empirical Lotz formula is used to calculate electron impact ionization probabilities [136], taking into account a correction of I_P due to the presence of other ions [29]. Ionization over excited levels is also implemented [137]. The recombination is treated naturally by three body recombination.
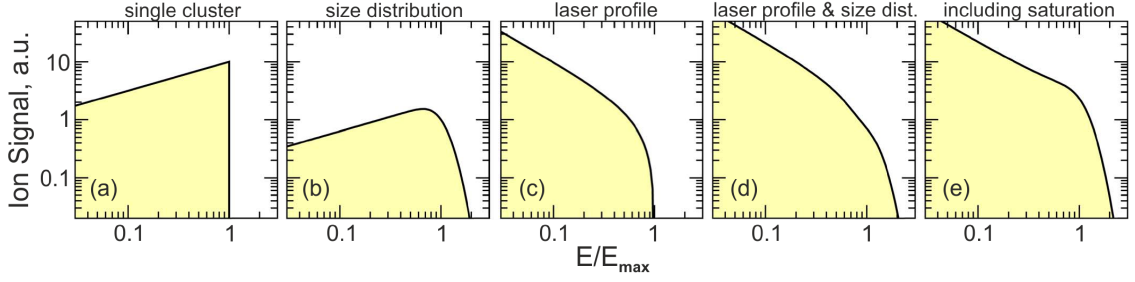
Figure 1.6.: Calculated ion energy spectra from the Coulomb explosion of clusters. (a) clusters of a certain size are exposed to a given laser intensity, Eq. 1.4; (b) the log-normal cluster size distribution is taken into account, Eq. 1.6; (c) considering a Gaussian laser profile; (d) size distribution and laser profile; (e) including ionization saturation. Adapted from [143].

Radiative recombination is calculated by applying corresponding rates. The electric field acting on each particle is a superposition of the external laser electric field in dipole approximation and the fields of other particles. Therefore, the computational costs scale propotionally to the square of the number of particles, which makes the simulation of the cluster with ion number $N_i > 10000$ practically inaccessible. In case of smaller clusters, the use of supercomputers is often necessary and a full simulation may last weeks. MD simulation allowed explanaition of many experimental observables, as electron emission spectra [26, 29, 47], ion charge state distributions [102], and ion spectra [108]. The advantage of the method is the possibility to trace the trajectories of the individual particles and resolve the acceleration mechanisms, e.g., plasmon-mediated electron acceleration in metal clusters [46].

For larger clusters, e.g., up to hundreds nm, particle-in-cell (PIC) simulations are used [21, 133, 135, 138–141], since the computational costs scale only proportionally to the particle number. Recently a microscopic PIC code corrected for hard collisions was developed [142]. Ionization is treated usually as in MD, but the fields are calculated by solving the system of Maxwell equations on a grid. This Ansatz automatically includes the field retardation and weakening of the laser field by absorption inside the cluster. The particle dynamics is treated by the solution of the equations of motion.

1.5. Ion recoil energy distributions from the Coulomb explosion of clusters

Separately, we consider a theoretical model developed by Islam et al. [143]. In contrast to other approaches discussed in Sec. 1.4, the interaction of clusters with the laser pulses is strongly simplified, but the laser intensity distribution in the focus and a realistic log-normal cluster size distribution are taken into account. The model can reasonably fit many experimental ion energy spectra [17, 107, 108, 144, 145] and illustrates how averaging over the focal volume and over the cluster size distribution cover the features of the single cluster response. In the model, a cluster is represented as an instantaneously uniformly charged sphere of constant density. The cluster explosion occurs solely due to the Coulomb

repulsion force. Then the probability P of an ion to have energy E is:

$$\frac{dP}{dE} = \frac{3}{2}\sqrt{\frac{E}{E_{max}^3}}\Theta(1 - \frac{E}{E_{max}}) \tag{1.4}$$

where E_{max} is a parameter corresponding to the maximal ion energy and $\Theta(x)$ is the Heaviside step function, which is 1 for $x \geq 0$ and 0 otherwise. The calculated ion energy spectrum is shown in Fig. 1.6, a. The signal grows with the recoil energy. The slowest ions originate from the cluster center and the ion energy increases with the distance from the center reaching E_{max} at the surface. To take into account the cluster size distribution, two assumptions are made: 1) the charge density in the cluster is independent of its radius and 2) the cluster sizes are distributed log-normally, i.e., the probability g that a cluster consists of N atoms is:

$$g(N) = \frac{1}{\sqrt{2\pi}\nu N}\exp\left(-\frac{\ln^2(N/N_0)}{2\nu^2}\right) \tag{1.5}$$

where N_0 and ν are the parameters of the distribution function. The average cluster size can be calculated as $\overline{N} = N_0 \cdot e^{\nu^2/2}$. Convoluting the single cluster ion energy spectrum Eq. 1.4 with $g(N)$ obtains the cluster size averaged ion spectrum:

$$\frac{dP_{size}}{dE} = \frac{3}{4}\sqrt{\frac{E}{E_{max}^3}}\text{erfc}\left(\frac{3\ln^2(E/E_{max})}{2\sqrt{2}\nu}\right) \tag{1.6}$$

where E_{max} is the maximum energy of ions from the clusters of size N_0 and erfc(x) is the error function. Eq. 1.6 will be used to fit experimental data in Appendix U. The calculated ion energy spectrum is presented in Fig. 1.6, b. The shape is similar to the result obtained for single clusters Fig. 1.6, a, but the spectrum is broadened. The ions with energies exceeding E_{max} stem from clusters larger than N_0. To take into account the averaging over the laser intensity distribution in the focus, the beam is assumed to have Gaussian spatial profile and the cluster charge density to be proportional to the strength of the electric field in the pulse. Fig. 1.6, c, shows the calculated spectrum for clusters of a single size. The envelope changes dramatically, i.e., here the signal decreases with energy. The strong contribution of low energy ions stems from the large volume in the focus, illuminated by lower I_{Las}. One can hardly draw a conclusion from the resulting spectrum about the shape of a single cluster ion energy distribution (Fig. 1.6, a). In Fig. 1.6, d, the result is presented when averaging over laser intensity and cluster size distributions is taken into account. The spectrum is similar in shape to Fig. 1.6, c, but even broader. In many experimental ion spectra, a high energy cut-off is observed, which is often called a "knee"-feature, see e.g., [145]. This feature can be well reproduced by the model if ionization saturation is assumed, i.e., the cluster charge density stays equal at laser intensities above some limit. The calculated spectrum is shown in Fig. 1.6, e.

In the current work, an intensity-difference spectrum technique is applied to minimize the effect of the focal averaging. The aim is to record spectra influenced only by the cluster

size distribution, e.g., as in Fig. 1.6, b.

2. Experimental methods

In this work, several new methods have been applied, which have not been used before to study the expansion of laser induced nanoplasmas. In particular, we developed charge-state resolving ion energy analyzer (CRIEA). The instrument is described in Sec. 2.1 and Publication A. Additionally, we applied an intensity-difference spectrum technique to overcome the signal averaging over the focal volume. We consider it in detail in Sec. 2.2. Other methods are introduced only briefly.

The experimental setup used in most of the studies is presented in Fig. 2.1. To produce strong NIR laser pulses two 1 kHz commercial laser systems were used: Spectra Physics, Model Solstice ($\lambda = 793$ nm, $E_{pulse} \leq 2.5$ mJ, $\Delta t \geq 130$ fs), and a combination of an oscillator (Femtolasers, Femtosource Synergy), acousto-optic modulator (Fastlite Dazzler) and an amplifier (Quantronics, Odin-II) ($\lambda = 810$ nm, $E_{pulse} \leq 1.2$ mJ, $\Delta t \geq 30$ fs). The laser radiation is focused by a lens ($f = 30$ cm) to a typically 30 μm diameter focal spot, reaching the intensity up to $I_{Las} = 1 \cdot 10^{16}$ W/cm^2. An attenuator based on a $\lambda/2$ plate and a pair of Brewster type polarizers (Altechna, Watt Pilot) is used to control the laser power. The pulse duration is measured by autocorrelators and third harmonic generation FROG*. We controlled the spatial profile of the laser beam by a CCD camera. In the double-pulse experiments a Mach-Zender interferometer was utilised.

To perform a measurement on rare gas clusters, an Even-Lavie pulsed source [68] installed on the constant flow cryostat was employed. A heating element provided precise temperature control. We placed the source approximately 40 cm away from the interaction
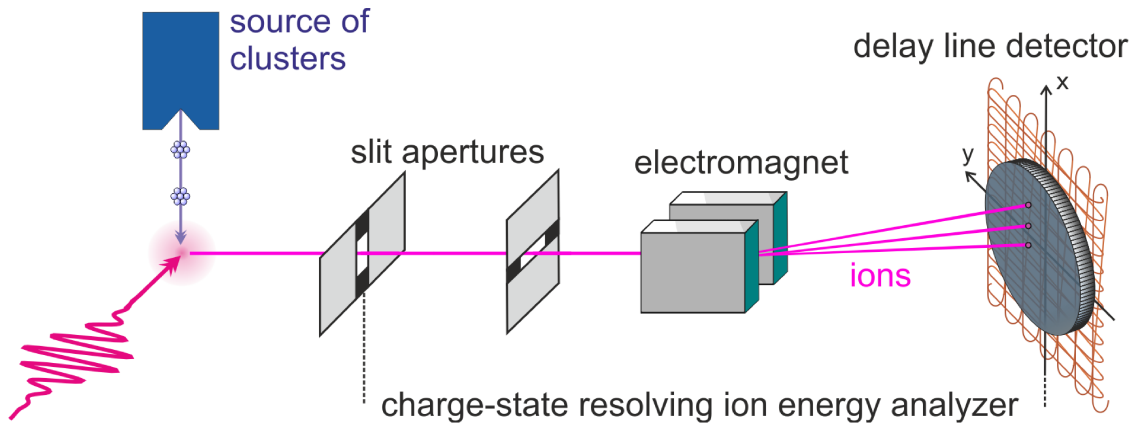

Figure 2.1.: Experimental setup to measure charge-resolved recoil energy spectra of ion emission from Coulomb explosion of clusters. Depending on the target, magnetron sputtering cluster source or Even-Lavie pulsed nozzle have been used. Experimental data presented in Sec. 3.2, 3.4, Manuscript C and Appendix U have been obtained with the setup.

---

*Frequency-resolved optical gating

point in a differentially pumped vacuum chamber to avoid effects due to the high cluster density [121–123]. Cluster sizes were estimated from Hagena scaling laws [65]. A detailed description of the setup and used parameters could be found in [146].

To produce metal clusters, a magnetron sputtering cluster source equal to the one described in [26, 47, 80] was employed. Since the cluster density in this case is several orders of magnitude less compared to Even-Lavie nozzle, the source output was placed only 5 mm away from the interaction point. The cluster mass distribution was controlled by a static quadrupole deflector, as described in [147, 148]. The velocity of the clusters was estimated by pulsing the voltage in the quadrupole and recording the time-of-flight signal with a detector based on a channeltron with a conversion dynode.

2.1. CRIEA: Charge-state resolving ion energy analyser (Publication A)

Typically, the Coulomb explosion of clusters is characterized by broad ion kinetic energy and charge state distributions, see Fig. 1.1. As mentioned above, simultaneous determination of charge and kinetic energy allows observation of correlations between expansion conditions during the laser pulse and subsequent recombination and relaxation. Thomson parabola spectrometers (TPS) which are commonly used for these reasons have a signifi-
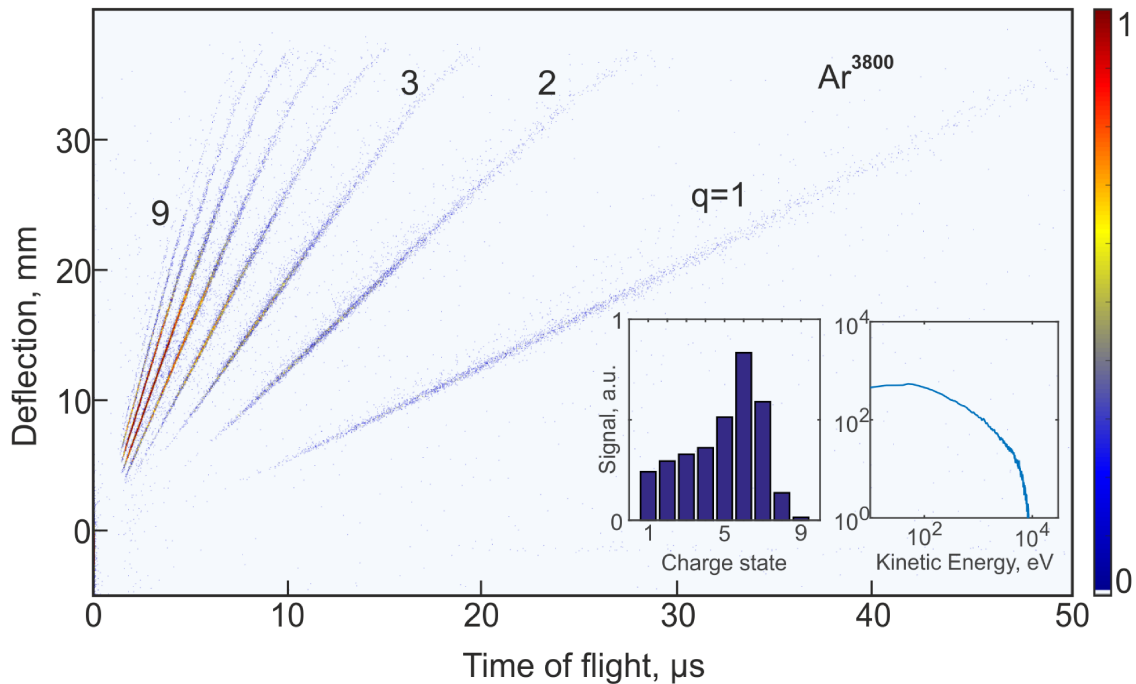
Figure 2.2.: A typical time-of-flight - deflection histogram recorded by CRIEA, obtained in an experiment on Ar-clusters exposed to $7.3 \cdot 10^{14}$ W/cm^2, 180 fs, 793 nm laser pulses. The lines correspond to signals from different ion charge states q. In the analysis time-of-flight spectra for each q are extracted, which allow recalculation of the charge-state resolved ion energy spectra, a charge-state distribution (left inset) or a recoil energy spectrum (right inset).

cant disadvantage, namely an extremely low transmission, e.g., on the order of 10^{-7}. Due to the high cluster densities produced by supersonic expansion sources, charge resolved ion energy spectra of rare gas clusters have been successfully recorded by this method [92]. Metal cluster sources produce streams with densities orders of magnitude lower, hindering measurements at sufficient resolution, see spectra in [40,93]. The charge-state resolving ion energy analyser (CRIEA) has been developed in this work to overcome this issue. CRIEA is a modification of a magnetic deflection time-of-flight spectrometer. We now shortly describe its operation principle. Ions emitted from the laser focal volume are collimated by the two slit apertures, pass through the region with a homogeneous magnetic field, and are detected by a position- and time-sensitive delay line detector, see Fig. 2.1. Resulting time-of-flight - deflection histograms are accumulated over many laser shots. An example is shown on Fig. 2.2. The signals of ions with equal charge state but different energies emitted from clusters form a line. Then for each line, a time-of-flight and corresponding energy spectrum are calculated. From one time-of-flight - deflection histogram, the charge state distribution, the recoil energy spectrum, and the charge resolved ion energy spectra may be extracted. We want to note that in contrast to conventional mass spectrometers, e.g., reflectron, in which the transmission decreases significantly with increasing ion recoil energy E_r, the transmission of CRIEA is practically E_r-independent. Hence, charge state distributions are measured with higher accuracy.

For a detailed description of the operation principle of a CRIEA, the analysis of the resolution, limitations, and additional examples see attached Publication A. Here we show only a short comparison of the instrument with a TPS, which has been optimized for laser-cluster experiments [92]. The advantages are:

- one to two orders of magnitude higher transmission due to the use of collimating slits instead of pinholes. The slit openings do not influence the energy resolution

- higher energy resolution since the energy is calculated from the time-of-flight, which can be measured with up to 100 ps precision

- broader energy ranges can be simultaneously measured due to the absence of an electric deflection field

- inhomogeneities of the magnetic field have only little influence on the energy resolution

Disadvantage is:

- the delay line detector can analyze typically only several tens of ions per laser shot. Therefore, spectrum has to be accumulated. This leads to unreasonably high accumulation times at repetition rates lower than 50 Hz.

2.2. Intensity-difference spectrum technique (IDS)

Due to the tight focusing of the laser radiation, the experimental spectra include signals from a broad laser intensity distribution. The features of the single cluster response are often completely smeared out, see Fig. 1.6. Since MD and PIC simulations even at a single laser intensity is time consuming, e.g., more then a day when using over thousand CPUs
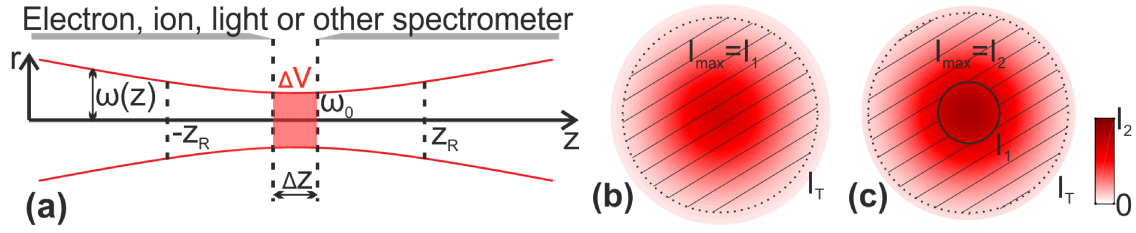
Figure 2.3.: (a) Schematic view of a typical strong laser field experiment on a gaseous target. The Gaussian laser beam is focused to a minimal diameter of ω_0. The volume accepted by the spectrometer ΔV is limited by the entrance slit. If the signal from the high intensity region is of interest, the slit opening Δz is usually significantly less then the Rayleigh length z_R. In (b) and (c), two intensity distributions across the beam cross section at maximum intensity I_1 and $I_2 = 1.2 \cdot I_1$ respectively are shown. The solid circle corresponds to I_1, the dashed – to $I_T = 0.1 \cdot I_1$. The hatched surface corresponds to the laser intensities between I_T and I_1. This surface is equal in each case. Keeping the laser beam diameter constant, an increase of the laser energy leads to the appearance of an additional surface in the cross section (inside the solid circle), corresponding to a high intensity, while the low intensity area is preserved. This method allows the user to define experimentally the response of the system to any intensity without focal averaging in only two measurements.

for a single run, the comparison of the calculated spectra to the experimental results may only be done qualitatively. Avoiding focal averaging in the data acquisition would provide a new quality of information about the single cluster response.

Since most of the strong laser systems emit light with a Gaussian spatial intensity profile, the geometry of the intensity distribution over the focus volume may be used to retrieve the target response to a single intensity from a series of measurements taken under different conditions. In the intensity selective scanning method, the intensity resolved signal is extracted from the measurements taken under different positions of the laser focus (z-scan) [149]. This technique was successfully applied on atoms [150] and small clusters [151–153]. In our experiments we keep the focusing system constant, but change the laser peak intensity by an attenuator, as was done in [31]. The method is called intensity-difference spectrum method. It allows determining intensity resolved spectra in only two measurements. Since the technique is new in the cluster community, we describe the method in detail below.

A schematic illustration of the interaction of strong laser radiation with a gaseous or cluster target is presented on Fig. 2.3, a. A laser beam with a Gaussian intensity profile is strongly focused by a lens or a focusing mirror. The laser intensity can then be described as:

$$I(r,z) = I_0 \left(\frac{\omega_0}{\omega(z)} \right)^2 exp \left(\frac{-2r^2}{\omega^2(z)} \right) . \tag{2.1}$$

where I_0 is maximum laser intensity, ω_0 is the beam waste and $\omega(z)$ is z-dependent beam diameter $\omega^2(z) = \omega_0^2(1 + (z/z_R)^2)$, where z_R is the Rayleigh length.

The axis of the analysing instruments is usually placed perpendicular to the laser propagation axis. To have a higher contribution from high laser intensity regions, the acceptance volume of the apparatus ΔV is often limited by the entrance slit, i.e., the opening Δz is smaller than the Rayleigh range z_R. For convenience, we assume $\Delta z \ll z_R$ so that the change of the laser beam diameter over Δz can be neglected, i.e., $\omega(z) = \omega_0$. This requirement is fulfilled in the experiments described in this thesis. The intensity distribution over the acceptance volume of the spectrometer is then described as:

$$I(r,z) = I_0 \exp\left(\frac{-2r^2}{\omega_0^2}\right) . \tag{2.2}$$

The volume dV exposed to some specific intensity I is then:

$$\left|\frac{dV}{dI}\right| = \frac{\pi \Delta z \omega_0^2}{2I} \qquad I \leq I_0 . \tag{2.3}$$

Clearly the volume dV exposed to some intensity I $(I \leq I_0)$ does not explicitly depend on I_0. That means, if the overall laser pulse energy is increased or decreased keeping the temporal and spatial profile of the laser pulse constant, e.g., by the attenuator, the volume exposed to the highest intensity is added or subtracted. An example is presented in Fig. 2.3 b, c. Increasing the on-axis intensity from I_1 to I_2 leads to the appearance of an additional high intensity volume (inside solid circle). The volume exposed to intensity I: $I_1 > I > I_T$ (hatched area) stays invariable, where I_T may be any intensity less than I_1.

In practice, the function of interest is the response function $R(I)$ of the target to a specific intensity I. If the target is homogeneously distributed over the volume and if laser-induced space charge effects are negligible, the signal $S(I_2)$ detected at peak intensity I_2 is

$$S(I_2) = \oint_{\Delta V} R(I)dV = \int_{I_T}^{I_2} R(I)\frac{\pi \Delta z \omega_0^2}{2I}dI . \tag{2.4}$$

where I_T is the threshold intensity that characterizes the onset of the target response. If we introduce an averaged response of the system $\langle R \rangle_{I_1}^{I_2}$ to intensities between I_1 and I_2, then

$$S(I_2) = \int_{I_1}^{I_2} R(I)\frac{\pi \Delta z \omega_0^2}{2I}dI + \int_{I_T}^{I_1} R(I)\frac{\pi \Delta z \omega_0^2}{2I}dI = \langle R \rangle_{I_1}^{I_2}\frac{\pi \Delta z \omega_0^2}{2}\log\left(\frac{I_2}{I_1}\right) + S(I_1)$$

$$\langle R \rangle_{I_1}^{I_2} = 2\left(\pi \Delta z \omega_0^2 \log\left(\frac{I_2}{I_1}\right)\right)^{-1}(S(I_2) - S(I_1)) . \tag{2.5}$$
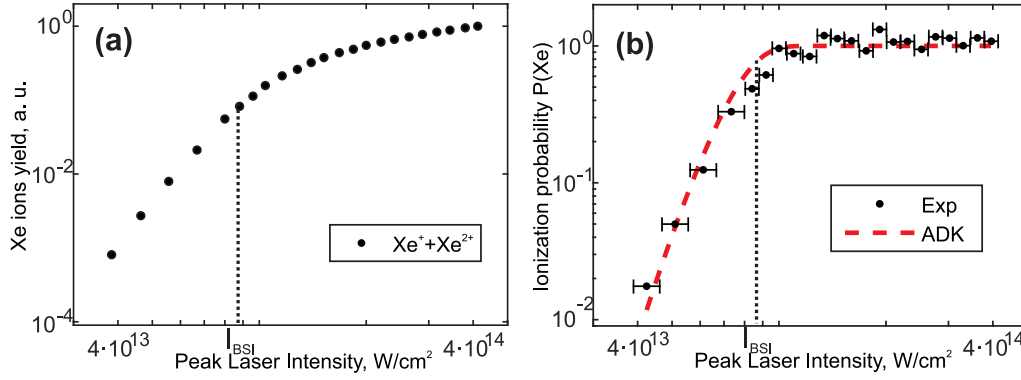
23

Figure 2.4.: (a) Experimental yield of $Xe^+ + Xe^{2+}$ depending on laser peak intensity. Due to the increase of the interaction volume, the yields increase even beyond the barrier suppression ionization threshold I_{BSI} (Eq. 1.2, dotted line). (b) Focal averaging as well as volume effects are cancelled out by the above described method of intensity-difference spectrum, which allows to determine the ionization probability $\langle P \rangle_{I_1}^{I_2}$ experimentally. Error bars show the limiting intensities I_1 and I_2. The red dashed line corresponds to the ionization probability calculated from ADK.

Hence, the difference of the spectra obtained at peak intensities I_2 and I_1 normalized to the volume equals the average specific response of the system to intensities between I_1 and I_2. Theoretically, $R(I)$ could be achieved by reducing $(I_2 - I_1)$ since $\lim\limits_{I_1 \to I_2} \langle R \rangle_{I_1}^{I_2} = R(I_2)$. Experimentally, it is necessary to keep the difference $(I_2 - I_1)$ high enough that $(S(I_2) - S(I_1))$ is still much larger than inaccuracies of the measurements.

The following requirements should be fulfilled to implement the method: (i) the spatial profile of the laser beam should be almost Gaussian; (ii) the target should be homogeneously distributed over the effective interaction volume; and (iii) signals from different parts of the interaction volume should not influence each other, e.g., space charge effects should be avoided. It is recommended to keep $\Delta z \ll z_r$, otherwise the signal at the intensities less than I_1 contributes to $\langle R \rangle_{I_1}^{I_2}$. Nevertheless, the contribution is still much lower than in $S(I_2)$ spectrum and can be calculated if the dependence of $\omega(z)$ is taken into account.

As a proof of principle we studied the ionization of xenon in the tunneling and barrier suppression ionization regimes. Xenon gas at a pressure of $1 \cdot 10^{-7}$ mbar was exposed to $\Delta t = 60$ fs $\lambda = 810$ nm laser pulses and ions were detected with a time-of-flight mass spectrometer. The ion yield is shown on the Fig. 2.4, a. Two reasons contribute to the growth of the signal: (i) the increase of the ionization probability with laser intensity and (ii) the growth of the interaction volume. The volume effect is obvious for intensities higher than the barrier suppression ionization threshold I_{BSI}. To de-convolute these contributions, we applied the method described above and we have chosen the ionization probability of Xe atoms $\langle P \rangle_{I_1}^{I_2}$ as an intensity specific response $\langle R \rangle_{I_1}^{I_2}$. The experimental results are presented in Fig. 2.4 (b) and compared to ADK model. The red dashed line shows the ionization probability calculated from ADK assuming $\Delta t = 60$ fs $\lambda = 810$ nm and pulse energies corresponding to 70 % of the energy used in the experiment. The experimental data agree well with the theoretical predictions. All volume effects as well as focal averaging effects were successfully cancelled out. A clear ionization saturation is observed at $I_{Las} > I_{BSI}$.

The reasons for the pulse energies correction can be reflections and absorption in the input window of the vacuum chamber, imperfection of the focus, and possible inaccuracies in the pulse duration measurements and/or ADK theory.

3. Outline of the results

As discussed in Chapter 1, many basic effects in the interaction of clusters with intense laser pulses have been described at least qualitatively. The aim of the current work is to extend the borders of knowledge in this field. In addition to the development of a charge resolving ion energy analyser, see Chapter 2 and Publication A, particular scientific challenges in the explanation of the laser-cluster interaction have been addressed in the framework of this thesis. The long-term relaxation of laser-induced nanoplasmas is discussed in Sec. 3.1 and Publication B. The asymmetric emission of ions from metal clusters excited in the impulsive regime was studied, see Sec. 3.2 and Publication C. In the last decade, many studies have been dedicated to the interaction of clusters with intense short-wavelength (e.g., XUV) radiation. Thus, the full characterization of the XUV-pulses from free electron lasers is of high importance. The results on the investigation of the spatio-temporal coherence of free-electron laser radiation in XUV by a Michelson interferometer are described in Sec. 3.3 and Publication D. Finally, yet unpublished results of the application of the intensity-difference spectrum technique on the interaction of metal and gas clusters with intense NIR-laser radiation are summarized in Sec. 3.4 and Appendix U.

The following sections include brief descriptions of the problems that have been raised, and highlight the results. The attached manuscripts and appendix contain detailed information about the applied methods, the experimental findings, and their discussions.

Published

3.1. Highly Charged Rydberg Ions from the Coulomb Explosion of Clusters (Publication B)

From the first laser-cluster experiments, an explanation of ion charge state distributions has been a challenge. If a full recombination of the quasifree electrons during cluster expansion is assumed, the calculated final ion charge states are well below those obtained in experiments [22]. Thus, the recombination and relaxation processes have to be considered in detail. MD simulations of nanoplasma disintegration into individual ions have shown that the majority of quasifree electrons, originally bound with hundreds of eV to nanoplasma, may not recombine into ionic core levels, but stay bound with low binding energies, e.g. below 50 meV [29], after cluster disintegration, see Fig. 3.1. The process is called frustrated recombination. It is assumed that these electrons may easily be removed by extraction or space charge fields, shifting the observed ion charge state distributions to higher values.

This study focuses on the recombination and relaxation of quasifree electrons in expanding nanoplasmas. If frustrated recombination takes place, an emission of ions carrying weakly bound electrons is likely. In order to experimentally resolve the presence of Rydberg electrons in the expanding nanoplasma, the CRIEA (Publication A) was extended by an extraction unit consisting of two electric field regions. When passing the field boundaries, ions with weakly bound electrons can be field-ionized and produce additional features in a time-of-flight - deflection histogram. The applied method analyses ions at a timescale greater than 50 ns after the laser excitation and is sensitive to a narrow charge-state dependent binding energy window, see Fig. 3.2, top.

We have performed measurements on argon clusters. For details, see Publication B. Ions
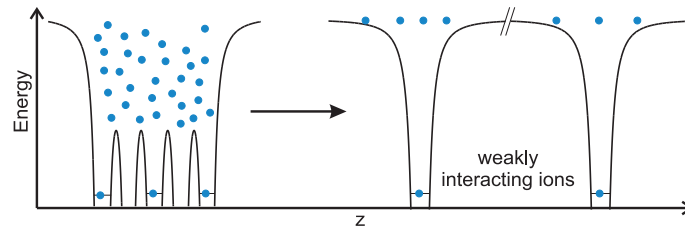
Figure 3.1.: Temporal evolution of a laser-induced nanoplasma. Left: directly after laser exposure, right: after plasma disintegration. During the adiabatic expansion of the plasma ball the delocalized electrons cool down and the mean field potential flattens. A majority of the initially hot electrons bound by the keV-deep plasma potential do not recombine into core levels but find themselves finally in low binding energy states (meV) of highly charged ions. Taken from Publication B.

Figure 3.2.: Top: Calculated charge state dependent binding energies of electrons in high-lying Rydberg levels of Ar^{q+} to be ionized by the electric fields of the extraction unit. The shaded area represents the energy window probed by the method. Lines are meant to guide the eyes. Bottom: Abundance of ions emitted from Ar_N undergoing autoionization (blue open bars) and field ionization (red filled bars). For both decay channels a considerable proportion of up to ten percent compared to the total signal is observed for each Ar^{q+}. The overall yields (dots) of these species account for a considerable fraction of the signal and peaks at about q = 5 giving a value of 15%. Adapted from Publication B.
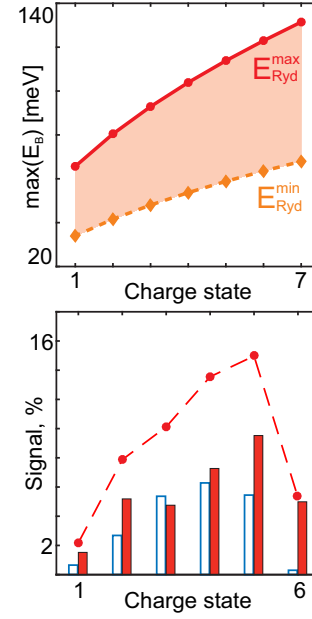
charged up to q = +8 have been detected. Ar^{q+} (q = 1-7) have been found to carry Rydberg electrons. Their yields are charge-state dependent and represent a significant part of the emitted ions. For example, about 10% of Ar^{5+} ions have an electron within a roughly 50 meV wide energy window, see red bars in Fig. 3.2, bottom. This is the first time that highly charged ions with electrons bound with such low energies have been observed. Hence, cluster Coulomb explosion serves as a source of these exotic particles. Additionally, our findings support the concept of frustrated recombination. It is likely quasifree electrons do not recombine to tightly bound ion levels, but instead appear to be weakly bound to the nanoplasma and recombine to high-lying Rydberg states. Limited by the experimental setup, we can assign the observed Rydberg electrons to $n_{Ryd} \geq 15$.

In addition to ions with Rydberg electrons, autoionization taking place on the flight to detector has been registered. An estimated timescale for the autoionization was found to be between 50 ns and several microseconds. A possible mechanism matching the timescale is the decay from autoionizing Rydberg states (ARS), which is a result of the Coulomb interaction between excited core and Rydberg electrons. The observed exceptionally long lifetime of ARS suggests that Rydberg states with high principle quantum number n_{Ryd} and high orbital quantum number ℓ_{Ryd} are generated.

3.2. Asymmetry of ion emission from metal clusters, excited in impulsive regime (Publication C)

In general, studies on ion emission from clusters exposed to ultrashort intense laser pulses report upon the predominant emission of fast ions along the laser polarization axis [43, 91, 107, 108], as discussed in Sec. 1.3.3. The development of laser systems with shorter pulse durations allowed study of cluster excitations in the so-called impulsive regime, when the laser impact is short enough to treat the ionic core as frozen during the ionization. This is typically realized at pulse durations below 50 fs. Two groups

have reported about a new, qualitatively different type of cluster explosion for impulsive excitation conditions. The ion emission exhibits so-called "unusual" asymmetry [30, 112], i.e., ions are predominantly ejected in the direction perpendicular to the laser polarization axis. Xenon and argon clusters have been investigated. Depending on the target and laser conditions, the energies or yields of ions may be enhanced in the perpendicular direction. The effect could be observed in MD simulations [115]; however, a direct comparison of theoretical results to the experimental findings have not been carried out. The following mechanism has been proposed as a possible explanation: under the influence of the laser field, the cloud of quasifree electrons is elongated along the laser polarization direction, providing a more efficient screening of the electric field on the cluster poles than on the equator. This effect leads to a more pronounced cluster explosion in the direction orthogonal to the laser electric field direction.

However, up to now experimental data are limited to only rare gas targets and selected laser parameters. The theoretical description that would quantitatively agree with the experiment is still absent. The aim of our study is to extend the available experimental data on laser-cluster interactions in the impulsive regime to metal clusters. In addition, utilizing CRIEA, contributions of each charge state in the asymmetric signal may be resolved. In our measurements, the laser parameters and cluster size have been chosen as in [30], when unusual asymmetry for both Ar_N and Xe_N is the strongest. The details of the experiment are presented in Publication C. We obtained ion spectra in parallel ($\theta = 0°$) and perpendicular ($\theta = 90°$) configurations, see Fig. 3.3, left. Charge states up to Ag^{9+} have been detected with energies up to 4 keV. In contrast to rare gas clusters, the emission is rather isotropic and the unusual asymmetry is not observed. Ions emitted in the direction along the laser polarization even gain slightly higher energies. Charge-state resolved energy spectra, see Fig. 3.3, right, show predominant emission of higher charged ions, e.g. Ag^{5+} and Ag^{7+}, along the laser polarization direction.

The obtained differences in the response of rare gas and metal clusters may not be intuitively
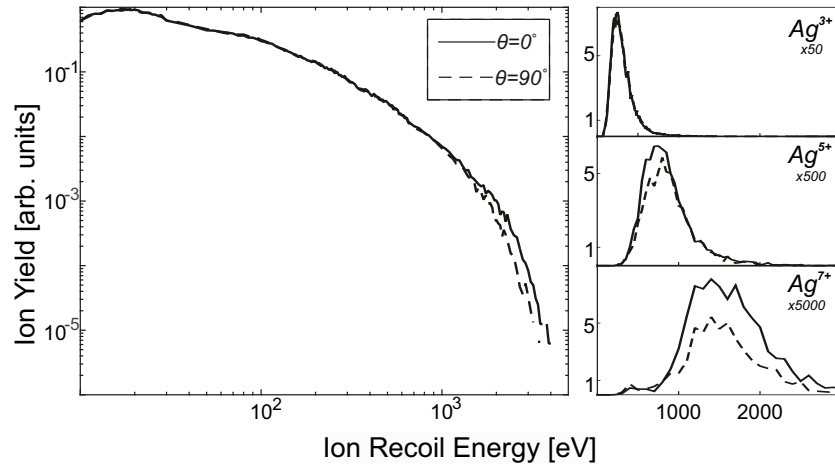

Figure 3.3.: Left: Ion energy spectra resulting from the interaction of 30 fs laser pulses ($I_L = 1.5 \cdot 10^{15}$ W/cm^2) with silver metal clusters N_{avg}=5000 recorded with parallel ($\theta = 0°$) and perpendicular ($\theta = 90°$) orientation to the laser polarization axis. Right: As left but charge-state resolved now. Taken from Publication C.

explained when we consider a mechanism such as proposed to be responsible for unusual asymmetry. The value of silver ion mass lies between Ar and Xe, so significant ion motion during the laser pulse is not expected. Ag has a lower I_P and is initially metallic, which may lead to an earlier onset of cluster ionization on the rising edge of the laser pulse. However, its influence is not obvious. We expect that our experimental results will motivate further investigations to clarify why a possible asymmetry in the ion emission should depend on the cluster material.

3.3. Spatio-temporal coherence of free-electron laser XUV radiation (Publication D)

An extension of the intense light-matter interaction studies to shorter wavelength radiation is of interest beyond the fundamental research, and opens up new possibilities in structural imaging of non-crystalline targets or even single particles, e.g., biomolecules or viruses [154]. Conducted with clusters, extreme ultraviolet (XUV) diffraction experiments at free-electron lasers (FEL) allows definition of structures of single silver nanoparticles [155] and intensity- and size-resolved measurements of the Coulomb explosion of rare gas clusters [156]. Moreover, imaging of dynamics in transient systems is possible, e.g., visualisation and trace of structural changes in the nanoparticles after optical excitation [157].

The analysis of XUV Thomson scattering may allow determination of transient temperature, density, and ionization in warm dense matter. We note that the resulting spectra allow determination of the above-mentioned plasma parameters without any assumptions from theory [158]. In 2013, a measurement campaign at FEL facility FLASH in Hamburg was conducted to study the time-resolved plasma properties of laser induced plasmas from hydrogen microdroplets. An intense NIR laser pulse ionized the target and a delayed XUV pulse probed the plasma. Together with a high throughput, high resolution spectrograph for soft X-ray light [159], which recorded the Thomson scattering signal, many diagnostic tools such as ion and electron spectrometers, have been utilized. Whereas the scattering spectra are still under discussion, the results obtained by one of diagnostic systems, namely an XUV spatio-temporal coherence analyser, led to a publication, see Publication 3.3.

When seeded by an external laser, a high coherence of the FEL radiation can be achieved [160]. Currently the FEL facility FLASH in Hamburg uses self-amplified spontaneous emission, which does not provide fully coherent radiation. The method considered in Publication D allows measurement of the spatio-temporal coherence of the laser beam. The technique is based on a Michelson interferometer, adapted to the XUV. By scanning an optical delay between the interferometer arms, the temporal coherence is measured by analysing the decay of the fringe visibility. In order to characterize the spatial coherence, a lateral shear is introduced. Different points of the wavefront are overlapping on the detector and the decay of the fringe visibility with the lateral displacement is used to extract the information about the spatial coherence. As a test, monochromatized FEL radiation of 13.5 nm was used. A temporal coherence time of (59 ± 8) fs was obtained, in a good agreement with the spectral bandwidth provided by the monochromator beamline. The spatial coherence in vertical and horizontal directions was found to equal 15 and 12% of

the beam diameter, respectively. The technique may be routinely utilized in FEL beamlines. When not monochromatized, a time coherence of about 3 fs has been reported by other studies [161–163].

Unpublished

3.4. Charge-state and intensity resolved ion energy spectra from cluster explosions (Appendix U)

The studies presented here and in the Appendix U focus on the explosion dynamics of laser-induced nanoplasmas and the formation of the final ion charge states. The charge state distributions and ion recoil energy spectra obtained in state-of-the-art experiments are averaged over different cluster sizes and laser intensities, as discussed in Sec. 1.2 and Sec. 1.5. Spectra corresponding to a given cluster size and a given I_{Las} are thus masked. The interpretation of the results is complex and often only a qualitative comparison to a theoretical predictions may be achieved. Additionally, only a few measurements on clusters have been conducted resolving ion charge states and energies simultaneously. Most of them focus on rare gas clusters, since they may be produced at high target densities and thus provide a higher signal rate. Previously, charge-resolved recoil energy spectra of metal clusters have been obtained, but only at a low resolution. Different charge states can not be unambigiously resolved [40, 93]. In this work, we use the instrument CRIEA, developed in the frame of this thesis (for details, see Sec. 2 and Publication A) and apply the intensity-difference spectrum method, see Sec. 2.2, to overcome the limitations in the signal analysis. Rare gas and metal clusters of different sizes have been studied.

In the focus of Appendix U are the first focal averaging-free measurements on the Coulomb explosion of nanoplasmas. Fig. 3.4 shows a comparison of charge state distributions (CSD) and recoil energy spectra (ES) with (c,d) and without (a,b) application of the intensity-difference spectrum technique. The intensity resolved CSD are significantly narrower then the focal averaged distribution. The intensity resolved ES differ in shape from the focal averaged spectrum. The application of the methods discussed above allows observation of effects that have not been identified in the previous experiments. With increasing laser intensity, the transition from partial to complete cluster explosion is resolved. Two different types of cluster explosion scenarios can be distinguished. At lower laser intensities, the surface of cluster is predominantly expelled, and the core expands significantly more slowly, i.e., so-called shell explosion - core expansion occurs. At higher intensities, clusters explode more homogeneously and may be represented as explosions of uniformly charged spheres. Further, the techniques allow one to experimentally distinguish thus far inaccessible parameters such as average ion recoil energies and average charge states. The comparison of the data to a simple model shows that, at least at certain laser intensities, quasifree electrons do not recombine to ions, i.e., our findings support the concept of frustrated recombination. At lower intensities, the charge-state resolved ion energy spectra show features of electron recombination. First MD simulations agree well with experimental results [164]. Further, we compare the ion emission from Ar_N and Ag_N under similar conditions. For silver clusters, a broad CSD spanning from Ag^{1+} to Ag^{15+}

Figure 3.4.: Focal averaged (top row) and intensity resolved (bottom row) charge state distributions (a,c) and ion recoil energy spectra (b,d) from Ar_{3800}, exposed to 180 fs NIR laser pulse of peak intensity $I_{Las} = 1.0 \cdot 10^{15}$ W/cm^2. The red line represent the optimal fit with the model of Islam et al. [143], Eq. 1.6. Negative values in (c) appears due to statistical oscillations of the signal in the experiment. Adapted from Appendix U.
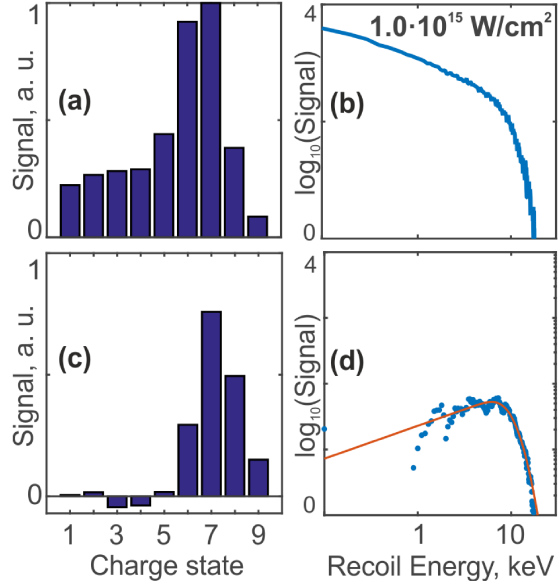
has been observed. In Ar_N, the CSD is significantly narrower. The origin of a narrow CSD in argon is most probably a combination of a transient resonance during the laser pulse and ionization saturation at Ar^{8+}. Finally, the role of the Mie resonance in the laser energy absorption was studied by a pump-probe excitation. An enhancement by more than an order of magnitude of ion recoil energies is observed under resonant conditions.

4. Summary and Outlook

The Coulomb explosion of rare gas and metal clusters induced by intense near-infrared femtosecond laser pulses was investigated. The temporal development including creation, expansion, and disintegration of the nanoplasma was studied by means of charge and energy resolving ion spectroscopy. Below we summarize the main achievements of the current work:

- A charge-state resolving ion energy analyser (CRIEA), optimized for laser-cluster experiments, has been developed, built and tested, see Publication A. The device features a one to two orders of magnitude higher transmission and a more than an order of magnitude higher energy resolution compared to other state of the art instruments. We demonstrated the capability of CRIEA to resolve charge states up to $q = 21$ and energies up to 300 keV from the Coulomb explosion of silver clusters. Operation with a dynamic range of 5 orders of magnitude has been demonstrated.

- The first high-resolution charge-state resolved ion energy spectra from metal clusters, irradiated by strong laser pulses have been obtained. The intensity as well as cluster size dependences of the ion emission were studied. We conducted charge- and energy-resolved studies of the dynamics with a pump-probe scheme for different cluster sizes. An increase in the ion recoil energies by more than an order of magnitude was observed by applying an optimal pulse delay.

- Studies of the ion emission asymmetry from silver cluster Coulomb explosion in the impulsive ionization regime have shown favourable emission of highly charged ions along the laser polarization axis and an isotropic emission of low-q ions, see Publication C. The result qualitatively differs from the observations obtained on rare gas clusters.

- A setup to realize measurements by applying intensity-difference spectrum technique has been assembled and tested. For the first time, intensity resolved spectra of the Coulomb explosion of clusters in the size range from 10 to 10^7 atoms have been obtained. The experimental findings allowed resolution of different cluster explosion regimes, e.g "shell-core" and "homogeneous".

- By comparing the obtained spectra with simple estimations, a robust experimental proof of frustrated recombination in clusters has been provided. Intensity resolved spectra may further serve as a benchmark to test theoretical models.

- A comparison of ion emission from the Coulomb explosion of argon and silver cluster under similar laser conditions has shown how element specific properties such as ionization potential, atomic mass, and cluster density influence the cluster ionization and subsequent heating and recombination in the nanoplasma.

- For the first time, highly charged ions with Rydberg electrons in the meV energy range have been detected, see Publication B. Our experimental results show that the

Coulomb explosion of clusters may serve as a source of these exotic particles. A quantitative measure of their yield in a specific binding energy range was obtained experimentally.

Outlook

In the future, a comparison of already obtained experimental results with advanced theoretical simulations, i.e. molecular dynamics or particle in cell, will likely provide additional insights about ionization, screening, and recombination in laser induced nanoplasmas. The application of CRIEA in experiments on many-body targets as clusters, biomolecules, nanoparticles, droplets, liquid jets, etc. would be of high interest. Charge state-resolved ion energy measurements would provide new insights in the ion acceleration processes. The intensity-difference spectrum technique (IDS) has demonstrated its huge potential for strong field nanoparticle research. Of high interest is an application of IDS on measurements with size selected particles. The results of such measurements would serve as a benchmark for theoretical models and would certainly allow to resolve the undergoing processes with higher accuracy. As a first exemplary target fullerenes may be used, since they have a well-defined structure and can be easily brought into the gas phase. In addition, the combination of IDS and phase-controlled $\omega - 2\omega$ pulses [26] may help to resolve and control electron dynamic on a sub-fs time scale.

Publications

A. High performance charge-state resolving ion energy analyzer optimized for intense laser studies on low-density cluster targets

D.Komar, K.-H. Meiwes-Broer, and J. Tiggesbäumker

The instrument, presented in the current publication, has been designed, constructed and tested by D. Komar. Further, D. Komar conducted measurements and analysed the experimental data. The manuscript has been written in team with the other co-authors.

B. Highly Charged Rydberg Ions from the Coulomb Explosion of Clusters

D. Komar, L. Kazak, M. Almassarani, K-H. Meiwes-Broer, and J. Tiggesbäumker

D. Komar planned the experiment and assembled the experimental setup. He conducted the measurements, analysed the data and contributed in writing the manuscript. L. Kazak set up the Even-Lavie cluster source. M. Almassarani assisted as a master student in assembling the experiment and performed some of the measurements under D. Komar's supervision.

C. No Substantial Asymmetries in the Ion Emission from Metal Cluster Nanoplasmas

D. Komar, R. Irsig, J. Tiggesbäumker, K.-H. Meiwes-Broer

D. Komar planned the experiment and assembled the experimental setup. He conducted the measurements, analysed the data and contributed in writing the manuscript. R. Irsig set up and operated the laser system.

D. Spatio-temporal coherence of free-electron laser radiation in the extreme ultraviolet determined by a Michelson interferometer

V. Hilbert, C. Rödel, G. Brenner, T. Döppner, S. Düsterer, S. Dziarzhytski, L. Fletcher, E. Förster, S. H. Glenzer, M. Harmand, N. J. Hartley, L. Kazak, D. Komar, T. Laarmann, H. J. Lee, T. Ma, M. Nakatsutsumi, A. Przystawik, H. Redlin, S. Skruszewicz, P. Sperling, J. Tiggesbäumker, S. Toleikis, and U. Zastrau

D. Komar participated in the setting up and conducting the NIR-pump – XUV-probe experiments on liquid hydrogen jets. In the measurements the collaboration focuses on imaging the time evolution of a warm dense matter target by recording the XUV-induced light scattering signals. The scattered light spectrum was measured in the perpendicular direction with respect to the laser beam axis by a high throughput, high resolution spectrograph for soft x-rays (HITRaX). In addition, an array of XUV diodes was used to record the angular distribution. In order to monitor, e.g., the hit statistic, a couple of additional diagnostic systems have been installed. The ion and electron signals have been recorded by time-of-flight spectrometers. For laser beam diagnostics a system of microscopes and light detectors was used to assure the spatial and temporal overlap of NIR and XUV pulses. A Michelson interferometer for XUV wavelengths has been installed to characterise the spatial and temporal coherence of the FEL radiation. Whereas the main results of the campaign are still under discussion, the data on the FEL coherence have been published. D. Komar contributed to the experiment by assembling the experimental setup, operating the time-of-flight spectrometer and analysing the ion spectra.

Appendix: Unpublished results

U. Charge state- and intensity-resolved ion energy spectra from cluster explosions

Here I present and discuss results on the interaction of clusters with NIR laser pulses ($\lambda_{Las} =$793 nm). Intensity-averaged as well as intensity-resolved ion spectra of rare gas and metal clusters are presented. The experimental methods used are described in the Chapter 2.

Argon clusters

We start the discussion of results with the analysis of ion signals obtained on argon gas clusters ($\overline{N} = 3800$, $R_{Cl} \approx 3.5$ nm) exposed to 180 fs laser pulses. Exemplary charge state distributions (CSDs) and spectra corresponding to different laser intensities are presented in Fig. U.1. Broad CSDs are observed. At $I_{Las} = 4.4 \cdot 10^{14}$ W/cm^2 (Fig. U.1, a), the distribution spans from $q =$1 to 7. The corresponding recoil energy spectrum (ES) spreads from zero to about 2 keV. Its shape qualitatively matches the spectrum predicted by the model of Islam et al. [143] (Fig. 1.6, d). At a higher intensity charge states up to $q =$9 are detected and a pronounced peak at $q =$7 is observed, see Fig. U.1, c. The corresponding spectrum, see Fig. U.1, d, spans up to 18 keV. In between $E =$10 and 20 keV the yield
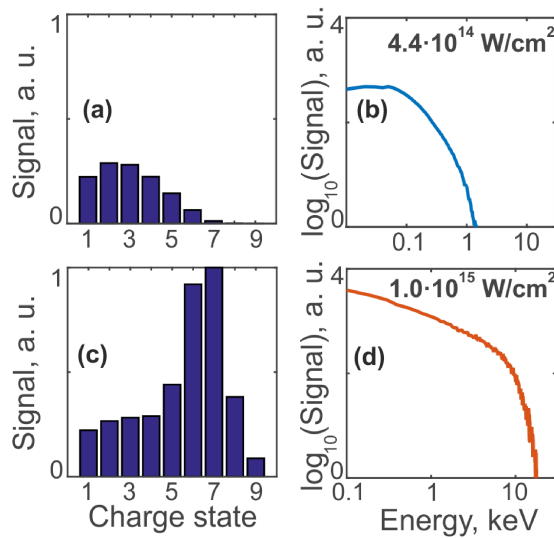

Figure U.1.: Charge-state distributions (a,c) and ion recoil energy spectra (b,d) at two values of peak laser intensity $I_{Las} = 4.4 \cdot 10^{14}$ W/cm^2 (blue) and $1.0 \cdot 10^{15}$ W/cm^2 (orange), respectively. Note different scaling in (b) and (d).
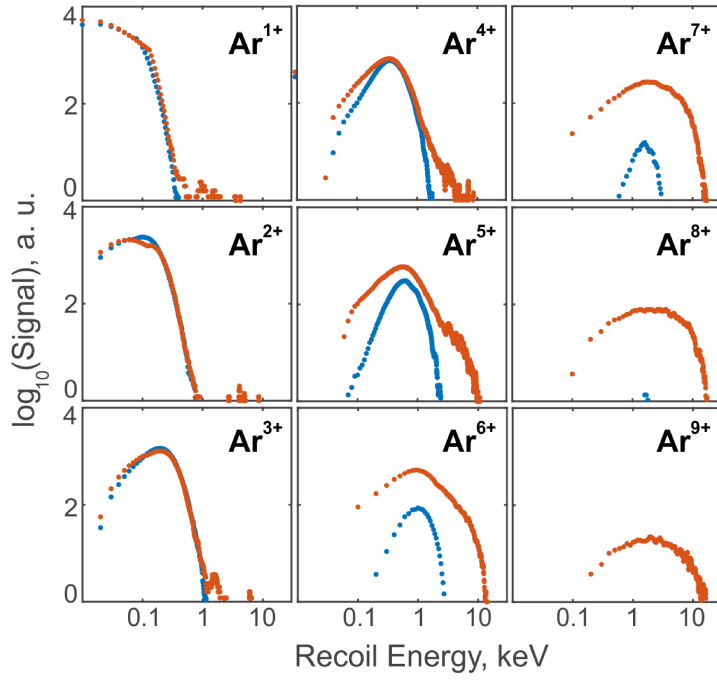
Figure U.2.: Charge-state resolved ion recoil energy spectra at two values of the peak laser intensity $I_{Las} = 4.4 \cdot 10^{14}$ W/cm^2 (blue) and $1.0 \cdot 10^{15}$ W/cm^2 (orange).

decreases by about two orders of magnitude, i.e., a pronounced "knee" feature is observed. The peak in the CSD is assumed to be an indication of ionization saturation: the charge state dependent ionization potentials I_P^{q+} show a pronounced step at Ar^{8+}, which results from a closed shell electronic configuration, see Fig. 1.5. During the laser pulse, cluster constituents are ionized up to charge state $q = 8$, but a further increase in q due to electron impact ionization requires significantly higher electron energies. Hence, for a range of laser intensities, the maximal charge state equals to $q = 8$. Experimentally, the distribution peaks at $q = 7$. We treat this as an indication of recombination (Ar$^{8+} + e \rightarrow$ Ar^{7+}) during the nanoplasma disintegration. The observation of a "knee" structure in the ion recoil spectrum supports the assumption made in [143], that this feature stems from ionization saturation.

The ion analyzer further allows resolution of the contribution of given charge states. Charge state resolved energy spectra are presented in Fig. U.2. They differ in shape from the total ion ES, see Fig. U.1, b, d. For $q = 1$ and 2, the spectra span down to zero kinetic energy. Higher charge states show pronounced energy cut-offs. For example, Ar^{7+} at $I_{Las} = 4.4 \cdot 10^{14}$ W/cm^2 has a low-energy threshold of $E^{min} = 600$ eV and a maximum energy of 3.1 keV. Some spectral shapes e.g., blue dots ($q = 4..7$), obviously cannot be represented as being the sum of q-dependent ion spectra stemming from homogeneously exploding charged spheres as assumed in the model of Islam et al., see Fig. 1.6, a. Non-trivial spatial charge distributions have to be assumed to reproduce the observed spectra, see below.

Although the laser intensities considered in Fig. U.2 differ by more than a factor of two, the energy spectra overlap for $q = 1..3$. Most likely, this is the result of focal averaging. As discussed in the Sec. 2.3, if the laser power is increased, an additional volume is illuminated by the higher intensity, while the volume illuminated by lower I_{Las} stays constant. Hence, if ions of selected charge states are not emitted from regions of stronger laser intensity, the
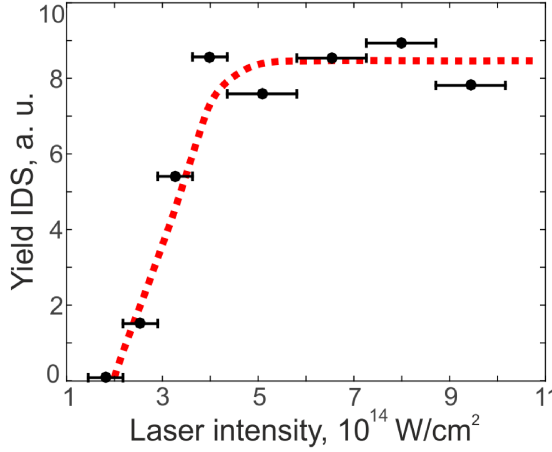
Figure U.3.: Intensity-resolved ion yields from Ar clusters as function of the laser intensity. Horisontal error bars indicate maximum and minimum laser intensity used to determine the intensity selective responce. The red dotted line serves as a guide to the eye. The observed saturation indicates that beyond $I_{Las} = 4 \cdot 10^{14}$ W/cm^2, the overhelming majority of cluster constituents are charged and have a recoil energy above the detection threshold of the CRIEA (10 eV in this measurement).

yields of these charge states show no increase at higher I_{Las}. Such a behaviour is observed for Ar^{1+} to Ar^{3+}, see Fig. U.2.

To overcome the effect of focal averaging, we apply the method of intensity-difference spectrum. Measurements have been conducted at different laser intensities and values of interest were analysed using Eq. 2.5. The results are marked in text with an acronym "IDS". Fig. U.3 presents intensity-resolved ion yields from Ar clusters as function of I_{Las}. A signal onset is obtained at $I_{Las} \approx 1.5 \cdot 10^{14}$ W/cm^2, which can be attributed to tunnelling ionization (Keldysh parameter $\gamma = 0.95$). At $I_{Las} \approx 4 \cdot 10^{14}$ W/cm^2, the ion yields saturate. This behaviour suggests that at intensities higher then $4 \cdot 10^{14}$ W/cm^2, all cluster constituents are charged and the clusters explode completely.

Spectra containing full information about ion emission from clusters exposed to a specific laser intensity are recorded by the CRIEA. Fig. U.4, a-d, shows IDS charge state distributions for selected laser intensities. The CSD attributed to partial cluster explosion is shown in Fig. U.4, a. It spans from $q = 1$ to 5, having a maximum at $q = 1$. Emission of a significant number of neutral atoms may also occur. However, they were not detected by the CRIEA since neutral atoms are not accelerated before the microchannel plate. Hence, a low detection efficiency is expected. In contrast, complete cluster disintegration is observed in Fig. U.4, b-d. The distributions peak at higher q. The signal of Ar^{1+} is negligible, which suggests that neutral atoms are not emitted. As expected, the IDS CSD are significantly narrower compared to normal CSDs, see Fig. U.1. The width of the distributions decreases with increasing laser intensity and average charge state, which takes place due to ionization saturation at $q = +8$.

The corresponding IDS ion ES are depicted in Fig. U.4, e-h. Their shapes are different when compared to the focal averaged spectra, e.g., Fig. U.1 (b,d). We fitted experimental data with the model of Islam et al. at a single laser intensity taking a log-normal cluster size distribution into account, see Fig. 1.6, b, and Eq. 1.6. A good agreement of the model with the experimental data is obtained. Eq. 1.6 includes three free parameters: N_0, ν and E_{max}, see Sec. 1.5. Fig. U.5 depicts the resulting values. N_0 increases with laser intensity and saturates at $I_{Las} > 6 \cdot 10^{14}$ W/cm^2. This behaviour reflects the transition from partial to complete Coulomb explosion which has been identified to occur at this I_{Las}. However, the saturation of N_0 is observed at slightly higher intensities when compared to the total ion yield, see Fig. U.3. The value of ν decreases with I_{Las} from $\nu = 3$ approaching

0.5 at intensities, when N_0 saturates. The observed trend strongly contradicts to the experiment, since in the measurements the cluster size distribution was kept constant. The discrepancy provides evidence that the model may not adequately represent the nanoplasma explosion in the studied laser intensity range. At $I_{Las} > 6 \cdot 10^{14}$ W/cm^2, where N_0 and ν saturate, the representation of the nanoplasma as a homogeneously charged sphere may still be valid. Higher values of ν at lower intensities suggest that the ion kinetic energy spectra are significantly broader then assumed in the model. Hence, one can conclude that at $I_{Las} < 6 \cdot 10^{14}$ W/cm^2, the charge distribution within the nanoplasma is strongly inhomogeneous leading to a much broader single cluster ion energy spectra compared to homogeneous charging, see Fig. 1.6, a.

In order to understand the cluster explosion dynamic in details we consider IDS charge-state resolved ion energy spectra. At $I_{Las} = 9.4 \cdot 10^{14}$ W/cm^2, see Fig. U.6 column (a), when we assumed homogeneous Coulomb explosion, the charge resolved ion spectra are quite similar to each other and can be well fit by the model of Islam et al. (size distribution only, Eq. 1.6). All four spectra were fit by using $\nu = (0.54 \pm 0.16)$ and $E_{max} = (8.6 \pm 0.5)$ keV. N_0 was adapted to each spectrum because of charge dependent ion yields. Since all spectra may be well fit with the same ν and E_{max}, we assume that, under considered laser conditions, the transient charge state distribution is narrow at the nanoplasma expansion stage, when ions gain most of the kinetic energy, and the electron cloud do not provide high charge gradient in the nanoplasma volume. That allows for a homogeneous expansion.

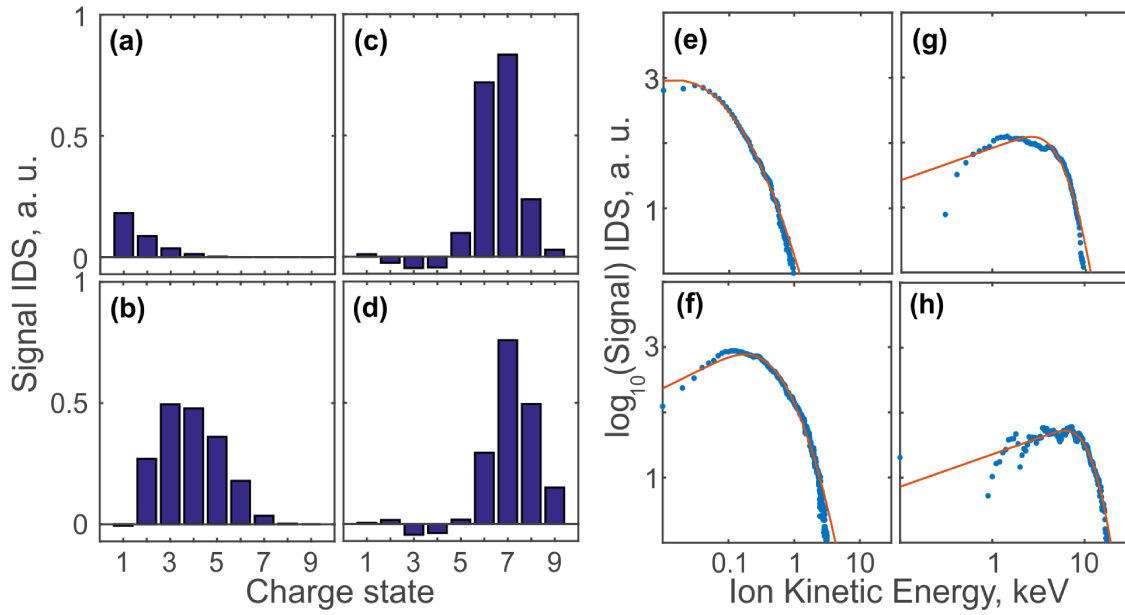In contrast, the envelopes differ strongly to each other at lower laser intensities ($I_{Las} =$

Figure U.4.: IDS ion charge state distributions and recoil energy spectra at different laser intensities: $I_{Las} = 2.5 \cdot 10^{14}$ W/cm^2 (a,e); $4.0 \cdot 10^{14}$ W/cm^2 (b,f); $6.5 \cdot 10^{14}$ W/cm^2 (c, g) and $9.4 \cdot 10^{14}$ W/cm^2 (d, h). See text for explanation. Values below zero in (a-d) appear due to experimental errors, e.g., imperfections of the laser beam profile or instabilities of laser and/or cluster source. Blue points represent experimental values in (e-h) and red lines represent the fit with a model of Islam et al. [143], Eq. 1.6. Note the different scaling in (e,f) than in (g,h).

$3.3 \cdot 10^{14}$ W/cm², Fig. U.6, column b). Only the signals of Ar¹⁺ and Ar²⁺ include signal at zero kinetic energy. Spectra of Ar⁴⁺ and Ar⁵⁺ instead show a peak structure and pronounced low energy cut-offs. Ions with low recoil energies are entirely absent. Obviously, the signal shape cannot be reproduced as a sum of single cluster ion energy spectra, as proposed by Islam et al. Fig. 1.6, a. We emphasize the strong dependence of E_{kin} on q. For instance, the spectrum spans up to 350 eV for $q = +1$, whereas at $q = +5$, maximum energy exceeds 1.5 keV.

The possible explanations of the observed peak structures in the ion spectra are: 1) Ions in higher charge states are produced only near cluster surface; 2) High-q ions are generated in the entire cluster volume, and highly charged ions from the core overcome the low-q ions and acquire additional energy by repelling from the sphere of lower charged ions; 3) The ions of higher charge states are produced throughout the cluster, but those produced in the core effectively recombine with quasifree electrons. Now we consider each possible hypothesis in detail.

1. Since the ionization within the nanoplasma occurs mainly due to electron impact ionization, previously there was no indication obtained, that ions on the cluster surface experience a significantly stronger ionization compared to core ions. When the asymmetry of ion emission from clusters was studied [43, 91, 108, 165], the small differences in the ionization have been attributed to the inhomogeneities of the spatial charge distribution in the oscillating cloud of quasifree electrons. However, these effects are too weak to explain the observed ion spectra. Therefore the first explanation can be excluded.

Figure U.5.: Laser intensity dependent parameters used to fit the experimental intensity resolved ion energy spectra with the model of [143]. (a) N_0 represents the average cluster size and the cluster gas concentration; (b) ν characterizes the width of the cluster size distribution; (c) E_{max} equals to maximal ion kinetic energy, emitted from clusters of the size N_0.
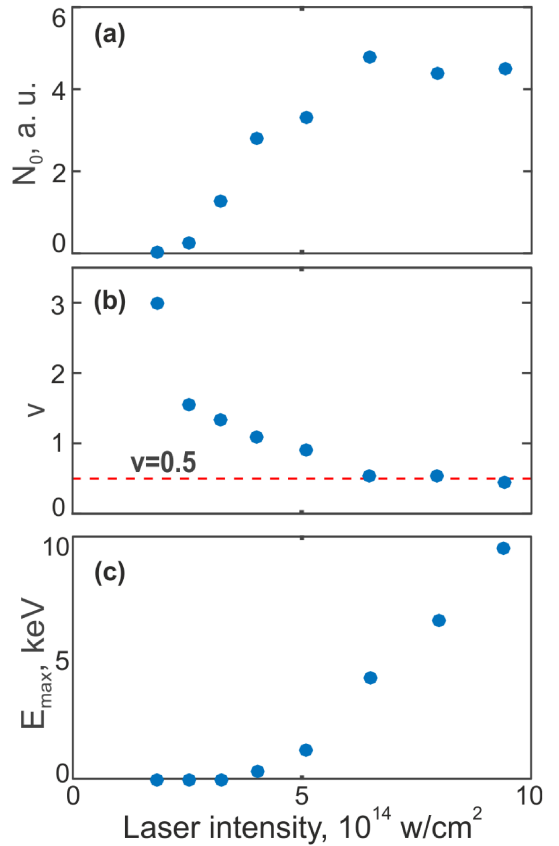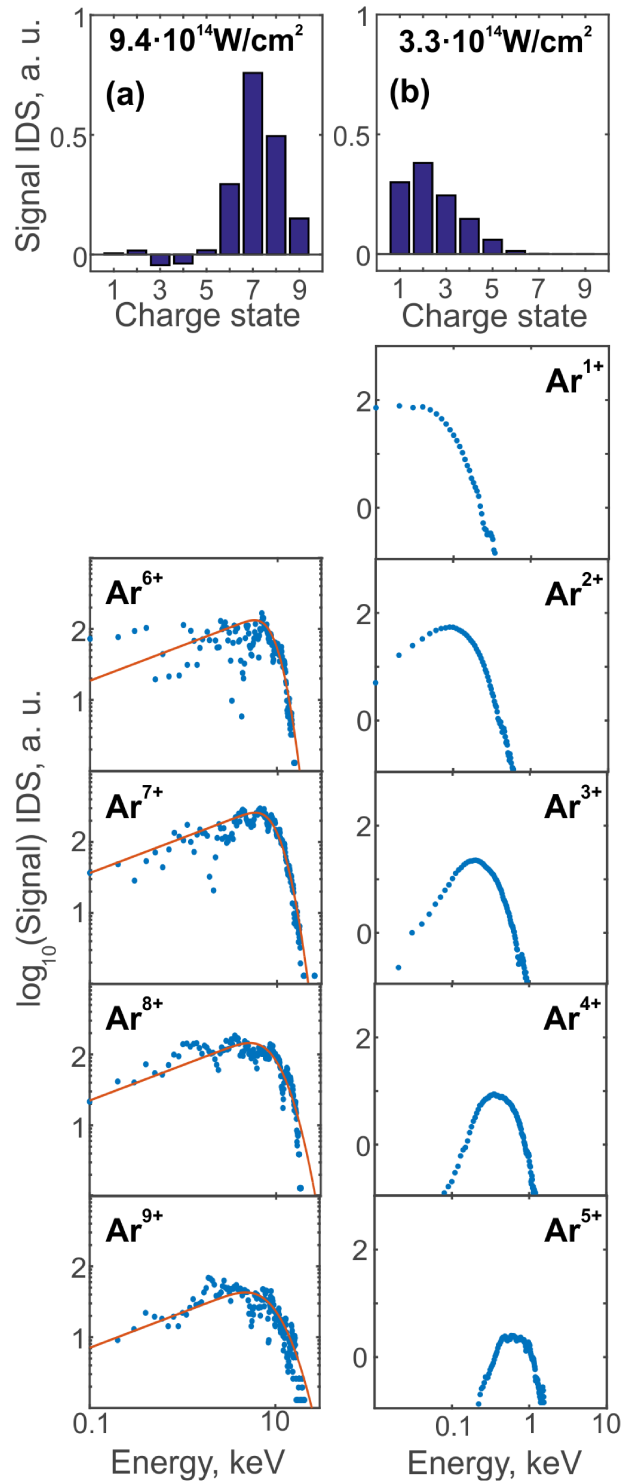
Figure U.6.: Column (a): IDS charge-state distributions and charge resolved ion recoil energy spectra at $I_{Las} = 9.4 \cdot 10^{14}$ W/cm^2. Blue points represent the experimental data, red lines - fit with the model of Islam et al., Eq. 1.6. Column (b): as (a), but at $I_{Las} = 3.3 \cdot 10^{14}$ W/cm^2. Note the different scaling.
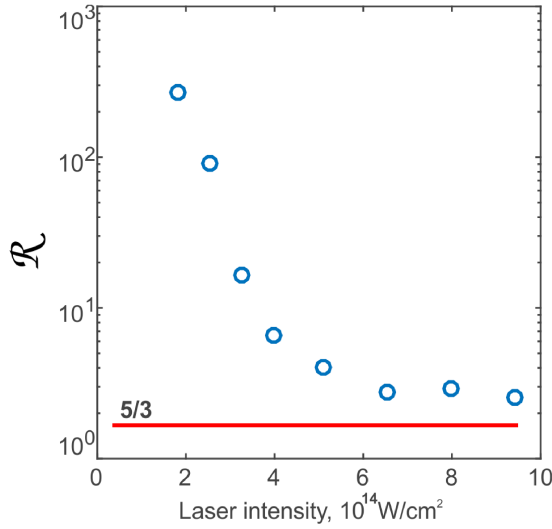
Figure U.7.: The ratio of intensity resolved maximum to average ion kinetic energy $\mathcal{R}$ as function of laser intensities. For the explosion of homogeneously charged spheres a value of $\mathcal{R} = 5/3$ is expected. The development of $\mathcal{R}$ with I_{Las} clearly shows the transition from a "shell-core" to a "homogeneous" nanoplasma explosion. Note the logarithmic scaling on the y-axis.

2. To strictly confirm or exclude the second hypotheses, a microscopic simulation of the nanoplasma expansion would have to be conducted, which goes beyond the scope of the thesis. Here we give only some arguments. The described scenario may be realised only if highly charged, e.g., Ar^{5+}, and lower charged ions or even neutral atoms are present in the cluster core, providing a huge difference in ion mobility. However, neighbouring ions in very different charge states would induce electron transfer, which would smooth out the charge distribution. Additionally, quasifree electrons would screen higher charged ions, reducing their effective charge state and, as result, the ion mobility. From these arguments, one can assume the second hypothesis is unlikely as well.

3. The third hypothesis, in contrast, does not imply a huge charge gradient inside the cluster and is consistent with the presence of a high number of quasifree electrons, which are essential for effective laser energy absorption. Moreover, previous studies on EUV-emission from core-shell clusters have confirmed a significantly higher recombination in the cluster core compared to the surface [166]. In studies on the ion emission from larger particles (R=180-600 nm), a similar peak structure in the charge-state resolved ion energy spectra has been observed. Corresponding MD simulation support the assumption of the recombination in the core ions [156].

As discussed above, at $I_{Las} < 6 \cdot 10^{14}$ W/cm^2 the ion kinetic energy distributions are broader as expected from the explosion of homogeneously charged spheres. As a measure of a non-uniformity we propose to use the ratio $\mathcal{R}$ of maximum to average ion kinetic energy. From simple electrostatic considerations one can show that $\mathcal{R}=5/3$ for a homogeneously charged sphere. The dependence on laser intensity $\mathcal{R}(I_{Las})$ is shown in Fig. U.7. At $I_{Las} < 6 \cdot 10^{14}$ W/cm^2 the resulting value $\mathcal{R}$ is significantly higher than 5/3, e.g., ≈ 90 at $2.5 \cdot 10^{14}$ W/cm^2, which illustrates a substantial kinetic energy difference between the fastest high-q ions, produced on the cluster surface, and ions, emitted from the interior of the cluster. At $I_{Las} > 6 \cdot 10^{14}$ W/cm^2, $\mathcal{R}$ levels out at about 8/3. The difference from 5/3 may appear, e.g., due to still-present charge gradient in the nanoplasma or the cluster size distribution.

This brings us to a first conclusion. The analysis of IDS-spectra reveals that the cluster

Figure U.8.: The ratio of the estimated nanoplasma radius R_{est} after the laser pulse to the initial cluster radius R_{init} (blue ●). The horizontal lines indicate resonant conditions at selected values of the average ion charge state in the nanoplasma $< q >$. It is highly probable that resonant conditions are transiently fulfilled at $I_{Las} > 4 \cdot 10^{14}$ W/cm^2.
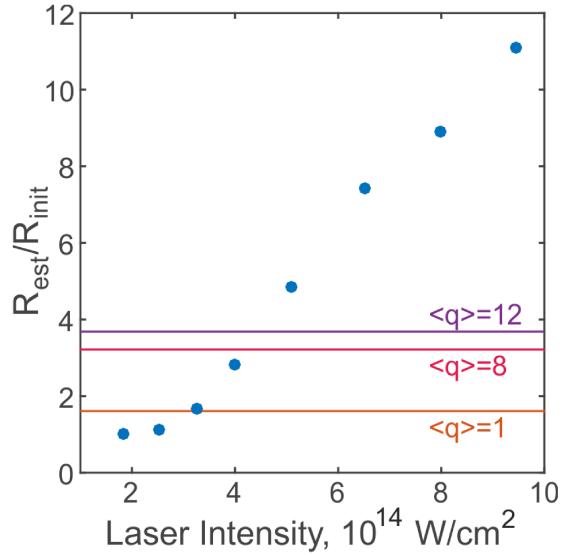
explosion dynamics strongly depends on the laser intensity, i.e., the absorbed energy. At $I_{Las} < 6 \cdot 10^{14}$ W/cm^2, the process can be represented as an explosion of the cluster surface, which carries a larger part of the uncompensated positive charge. Screened by the quasifree electrons, the cluster core expands significantly slower. With increasing laser intensity, the nanoplasma explodes more homogeneously and may be represented as a uniformly charged sphere. In other words, we observe a transition from "surface explosion, core expansion" to "homogeneous nanoplasma explosion".

Next we consider the intensity dependent laser energy absorption by analyzing the ion kinetic energy release. The dependence of the fit parameter E_{max} on the laser intensity is obviously super linear, see Fig. U.5, c. The dependence of the average ion kinetic energy on I_{Las}, shown in Fig. U.9, a, confirms this trend. As discussed in Sec. 1.3.2, efficient energy absorption in clusters takes place when the laser frequency matches the Mie frequency, see eq. 1.3. At the initial density of solid argon and an average ion charge state $< q >= 1$ calculated λ_{Mie} equals 389 nm. Hence, the ion density is too high to excite the resonance with $\lambda_{Las} = 789$ nm. Since the cluster expands during the laser pulse, resonant conditions may still be transiently fulfilled. To calculate the time-dependent ion density $n_I(t)$ and the average charge state $< q > (t)$, MD or PIC simulations are necessary. However, one can roughly estimate the expansion during the laser pulse by applying a simple model. We assume the cluster to be a uniformly charged sphere with an initial radius $R_{init} = r_{WS} \cdot N^{1/3}$, where r_{WS} is the Wigner-Seitz radius. The expansion is assumed to occur solely due to Coulomb repulsion force. The cluster is instantly charged in such a way that after the explosion, the resulting average kinetic energy equals the kinetic energy observed in the experiment. Next, we solve the equations of motion and calculate the nanoplasma radius R_{est} after a time equal to the laser pulse duration. The result is presented in Fig. U.8. Horizontal lines mark calculated values corresponding to resonance radius for $< q >= 1$, 8 and 12, respectively. Already at $I_{Las} > 4 \cdot 10^{14}$ W/cm^2 resonant conditions may occur. This intensity corresponds to the onset of full cluster disintegration, see Fig. U.3, and efficient energy absorption, see Fig. U.5, c, and Fig. U.9, a. Therefore, it is highly probable that efficient energy capture at the considered conditions indeed happens because of the resonant absorption by the collective oscillation of the quasifree electrons.
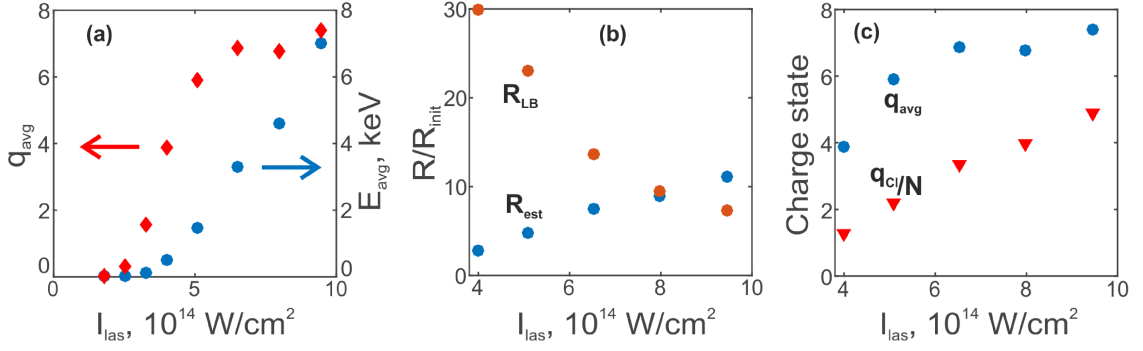
Figure U.9.: (a) Average charge state (red ◇) and average ion recoil energy (blue ●) as function of laser intensity. (b) Estimated lower boundary of the nanoplasma radius R_{LB} assuming a full recombination of the quasifree electrons (orange) and the estimated cluster expansion R_{est} during the laser pulse (blue) as a function of I_{Las}. This example shows the inconsistency of the assumption of full electron recombination. (c) Intensity dependent experimental average ion charge state q_{avg} (blue) and calculated ratio of nanoplasma charge-to-ion number q_{Cl}/N (red). q_{avg} and q_{Cl}/N estimate the number of quasifree electrons in the nanoplasma and the amount of recombined electrons. See text for explanations.

The combination of the CRIEA and IDS allows experimental determination of laser intensity dependent average ion charge states q_{avg} and average ion kinetic energies E_{avg}. The results are present in Fig. U.9, a. The two curves express significantly different behaviour. Above $I_{Las} = 5 \cdot 10^{14}$ W/cm², q_{avg} starts to saturate, but E_{avg} increases further. When q_{avg} grows by 25%, E_{avg} enhances by a factor of five. Since the Coulomb repulsion is one of the main driving forces in the nanoplasma explosion, this behaviour is rather counter-intuitive. In order to rationalize these observations, we model the nanoplasma as a uniformly charged sphere, which explodes due to Coulomb repulsion exclusively. We assume that in the laser excitation at a certain time the nanoplasma charges up to a charge $N \cdot q_{avg}$. This assumption is equal to the assertion that after that time no further ionization takes place until we register the charge state distribution. We may estimate the lower boundary of the nanoplasma radius R_{LB} at which this charging occurs as following:

$$R_{LB} = \frac{3}{5} \cdot \frac{e^2}{4\pi\varepsilon_0} \frac{q_{avg}^2 N}{E_{avg}} \tag{U.1}$$

The dependence of R_{LB} on I_{Las} is presented on Fig. U.9, b, (orange ●). For comparison the values of the previously estimated nanoplasma radius R_{est} after the laser pulse are shown in blue. At $I_{Las} < 7 \cdot 10^{14}$ W/cm², R_{LB} is larger then R_{est}. Hence, a significant outer ionization of the nanoplasma has to take place after the interaction with the laser pulse. This may occur only if some of the quasifree electrons, which are bound to the nanoplasma during the laser pulse, never recombine. In other words, our experimental results support that recombination of quasifree electrons is frustrated at least in some laser intensity regimes, as predicted in [29]. This leads to a shift of the observed charge state distribution to higher values.

As discussed in Sec. 1.3.2, the strongest ionization and heating of the nanoplasma takes

place at the critical density. One can roughly estimate the charge of the nanoplasma including quasifree electrons. To do this, we model the nanoplasma as a homogeneously charged sphere with a corresponding to resonant conditions radius R_{Mie} and disregard the ion kinetic energy acquired before resonance. Neglecting the hydrodynamic pressure of the electrons, the total cluster charge can be estimated from electrostatic considerations as:

$$\frac{q_{Cl}}{N} = \sqrt{\frac{5}{3} \cdot \frac{4\pi\varepsilon_0}{e^2} \frac{E_{avg}R_{Mie}}{N}} \tag{U.2}$$

where E_{avg} is the experimentally obtained average ion energy. Note that Eq. U.2 rather overestimates q_{Cl}/N. It is reasonable to calculate q_{Cl}/N only at laser conditions, when the plasmon resonance can be achieved. The results are presented in Fig. U.9, c. Experimental q_{avg} are shown for comparison. q_{Cl}/N is indeed much lower then q_{avg}. Assuming that the ionization in clusters is saturated at the resonance, i.e., the ions are in transient charge state $q_{sat} = +8$, the difference $q_{sat} - q_{Cl}/N$ may be used as an estimation of the number of quasifree electrons. The difference $q_{sat} - q_{avg}$ indicates the number of quasifree electrons that actually recombined.

Fig. U.9, c, shows that the nanoplasma expansion occurs in the presence of a quasifree electron cloud even at the highest laser intensity. How can one explain a "homogeneous" explosion? Most likely, the explosion is non-uniform, but at high laser intensities the "inhomogenity" is low enough to be covered by the cluster size distribution and statistical fluctuations of the signal. At lower I_{Las} the "inhomogenity" seems to be stronger. Probably, the difference arises due to different efficiency of screening of core ions by quasifree electrons. The screening efficiency in plasmas in local thermal equilibrium is characterized by the Debye length λ_D. For a dense plasma exposed to a fast oscillating field λ_D may be calculated as follows [167]

$$\lambda_D = \sqrt{\frac{2\varepsilon_0}{3e^2} \frac{E_{avg}^{el}}{n_e}} \tag{U.3}$$

where E_{avg}^{el} is the average electron kinetic energy and n_e is the electron density. Eq. U.3 should describe the general trend, although the nanoplasma is far from thermal equilibrium. With increasing laser intensity, we expect a higher E_{avg}^{el}, which in turn increases λ_D. Since we have identified that ionization saturation occurs at Ar^{8+}, the total number of electrons is limited. At higher laser intensities, outer ionization increases and the cluster expands faster. Both these factors will result in a decrease of n_e and an increase of λ_D. Assuming an initial cluster radius, one quasifree electron per ion, and a reasonable value of 10 eV for electron kinetic energy, one calculates $\lambda_D = 1.3\text{Å}$, which is less then the Wigner-Seitz radius of Ar. However, at resonance, assuming four quasifree electrons per ion and 300 eV electron kinetic energy, λ_D equals 2 nm, which is about 2.9 times higher then an average distance between ions. Hence, the cloud of quasifree electrons screens the ion core less effectively with increasing energy absorption. As a consequence, a lower charge gradient is present in the nanoplasma and a more homogeneous explosion takes place.

The proposed analysis gives only a qualitative explanation. More precise information about electron screening and recombination in the expanding nanoplasma may be obtained
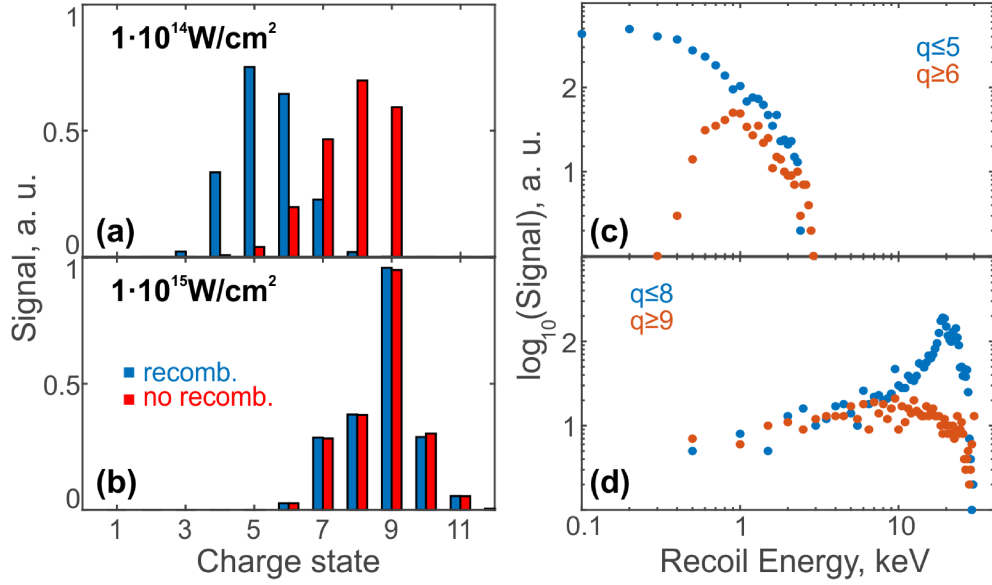
Figure U.10.: Results of MD-simulations on the explosion of Ar_{3871} clusters, exposed to 180 fs, $\lambda_{Las} = 793$ nm pulses at $I_{Las} = 1 \cdot 10^{14}$ W/cm^2 (a,c) and $1 \cdot 10^{15}$ W/cm^2 (b,d). Charge state distributions are shown in (a,b) with (blue) and without (red) electron recombination. (c,d) are the corresponding ion recoil energy spectra for selected charge states. Simulations have been conducted by Thomas Fennel.

by a comparison of the experimental results to more elaborate theoretical simulations. Taking the obtained data as a starting point, the group of theoretical cluster physics and nanophotonics at the University of Rostock has conducted the corresponding MD simulations. Preliminary results are shown in Fig. U.10. The MD code has been described in [29]. The plots (a) and (b) show charge state distributions for selected laser intensities. Red bars depict the transient charge state distribution whereas blue bars show the charge state distributions after recombination. Fig. U.10, c,d, depicts the corresponding ion recoil energy spectra. The simulated spectra are in qualitative agreement with the experimental data. At lower I_{Las}, recombination reduces the observed q_{avg} from 7.8 to 5.4, whereas at higher laser intensities recombination is frustrated. In the recoil energy spectra (Fig. U.10, c) low energy ions with $q \geq 6$ are absent, which provide evidence for recombination in the cluster core. In Fig. U.10, d, signatures of recombination are absent.

Silver clusters

To see how element-specific properties influence the cluster explosion dynamics, measurements with silver clusters have been conducted. We used the same laser system but with shorter pulses of 130 fs. The peak laser intensity was limited to $I_{Las} = 6.5 \cdot 10^{14}$ W/cm^2, otherwise strong signals from the processing gas of the cluster source (argon) saturate the detector. Intensity resolved ion yields as a function of laser intensity for four different values of average cluster size are shown in Fig. U.11, b-e. Typically, ion signal can be obtained beyond $I_{Las} \approx 1.5 \cdot 10^{13}$ W/cm^2. The Ag data are more noisy than these obtained for argon clusters (top row), since magnetron cluster aggregation is in general less stable
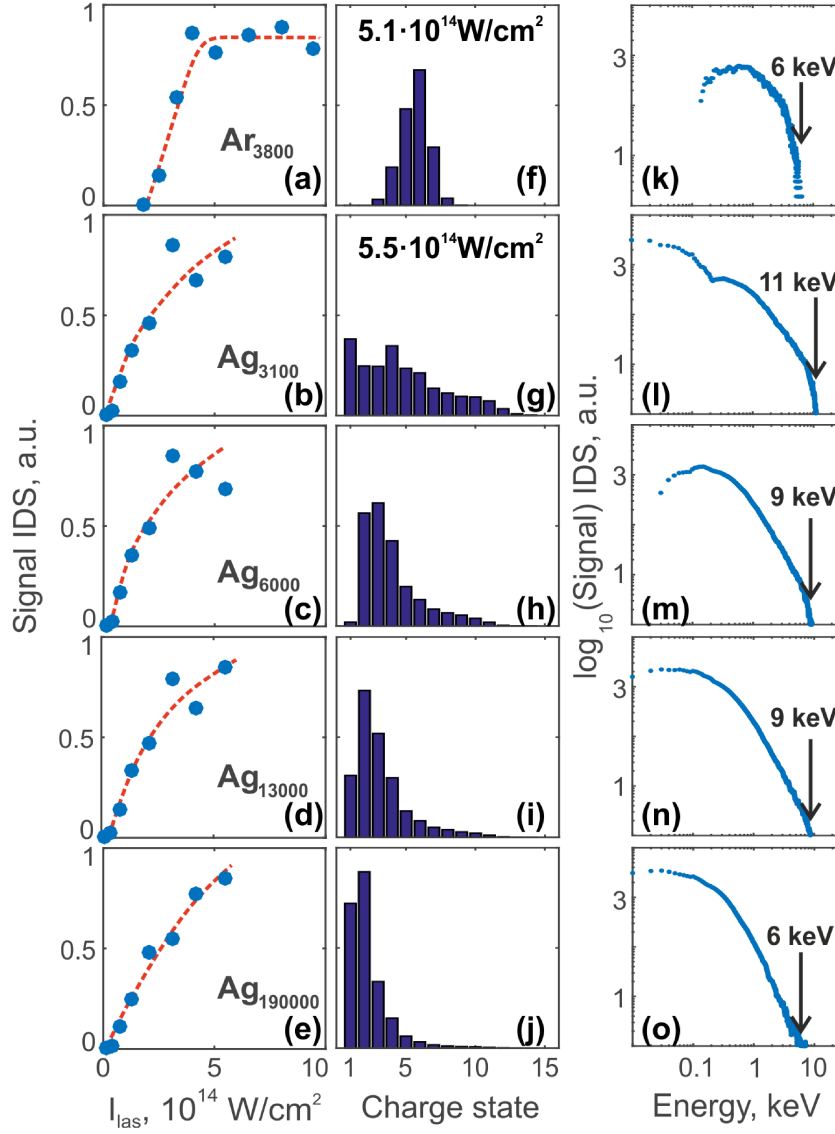
Figure U.11.: IDS total ion yields as a function of I_{Las} (a-e), IDS charge state distributions (f-j) and IDS recoil energy spectra (k-o). The data presented in each row correspond to a specific cluster material and an average cluster size. Note that results on Ar_{3800} are shown in the first row, whereas the results obtained on Ag_N are summarized in the lower rows. Data in (f,k) are obtained with 180 fs $I_{Las} = 5.1 \cdot 10^{14}$ W/cm^2 laser pulses, and in (g-j) and (l-o) with 130 fs $I_{Las} = 5.5 \cdot 10^{14}$ W/cm^2. In (k-o), the numbers denote maximum recoil energies.

Figure U.12.: IDS charge-state resolved ion recoil energy spectra for selected charge states, obtained by exposure of Ag_{3100} clusters to pulses of $I_{Las} = 5.5 \cdot 10^{14}$ W/cm². The envelopes of the spectra are characteristic for a "shell-core" cluster explosion. Observed signal drops, e.g., for Ag^{1+} and Ag^{2+}, appear because of statistical fluctuations in experiment.
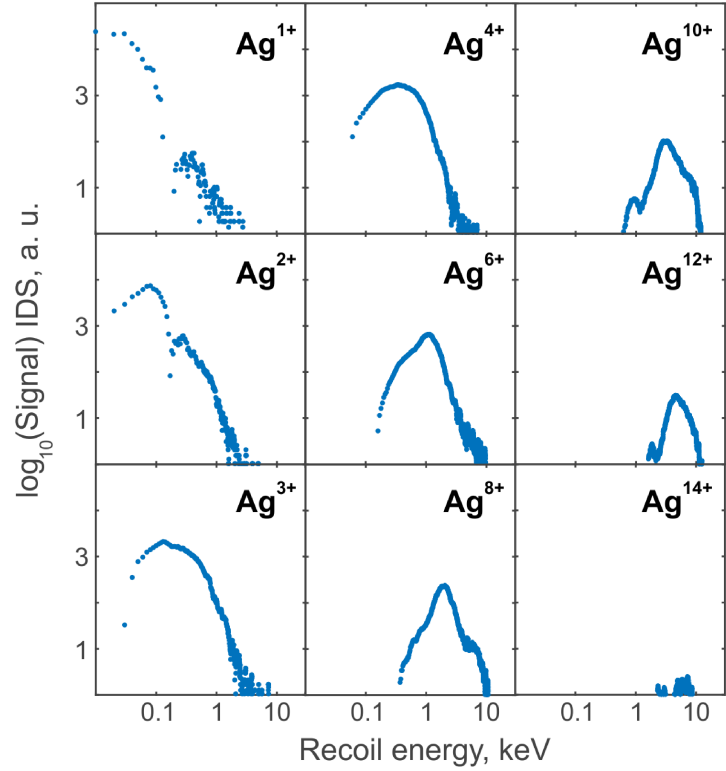
compared to supersonic gas expansion. The Ag^q-signals increase much more slowly with I_{Las} then those of argon clusters. In the whole intensity range studied, signal saturation was not observed for all four cluster sizes. Hence, only partial cluster disintegration occurs. Charge state distributions corresponding to the highest applied laser intensity are shown in Fig. U.11, g-j. Broad CSDs are observed, which span from q=0 to about 15. However, each of the distributions peak at q<5. Emission of neutral atoms and fragments is thus expected. This contrasts strongly with observations on argon clusters, for which complete cluster disintegration with a narrow charge state distribution has been observed. Additionally, a cluster size effect can be identified. For smaller clusters, e.g., Ag_{3100}, the charge state distribution is shifted to higher charge states compared to larger clusters, e.g., Ag_{190000}. The maximum recoil energies, see Fig. U.11, l-o, depend on a cluster size as well. Note that ions emitted from smaller clusters achieve higher kinetic energies. This trend contrasts with previous studies on rare gas clusters [14, 88, 144, 145] and will be discussed below.

Since the ionization potential of silver is significantly lower (7.58 eV) than that of argon (15.76 eV) [100], the ion signals from Ag_N show up at lower laser intensity compare to argon. $I_{Las} \approx 1.5 \cdot 10^{13}$ W/cm² indeed corresponds to the barrier suppression ionization threshold. As discussed above, when cluster constituents are ionized, the laser energy is mostly absorbed by quasifree electrons and the absorption efficiency strongly depends on λ_{Mie}. Assuming an average ion charge state of $q = 1$ and an initial cluster density corresponding to unexpanded cluster, one would obtain $\lambda_{Mie} = 237$ nm according to the Drude model. Hence, initially silver clusters are further out of resonance compared to argon. Due to the higher ion mass, the core expands slower and no resonant enhanced absorption is obtained under the given conditions, see below. Most likely, insufficient cluster heating is the reason for the observed incomplete disintegration of silver clusters.
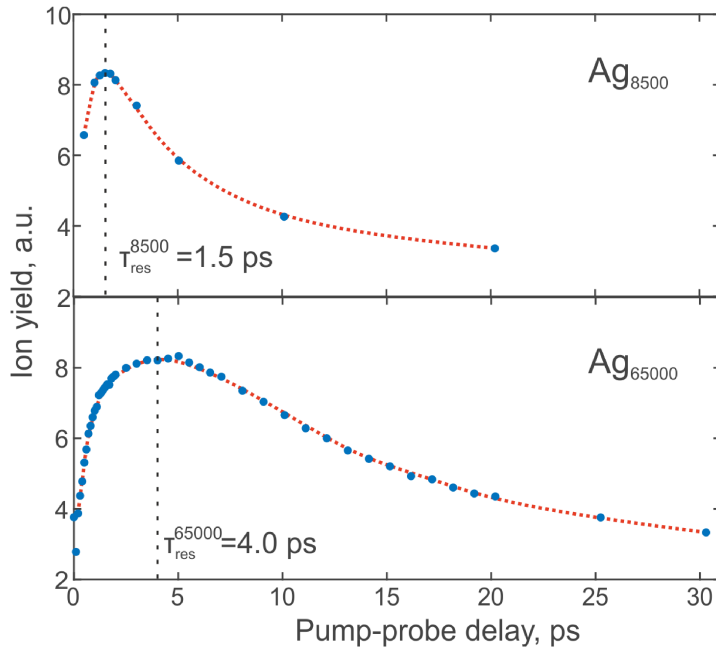
Figure U.13.: Total ion yields as function of the optical delay between pump and probe pulses τ for two values of $\overline{N}$. The peak in the signals correspond to conditions, when $\lambda_{Las} = \lambda_{Mie}$.

The broad charge state distributions, e.g., Fig. U.11, g-j, may partially be explained by the low I_P of silver, see Fig. 1.5. Further the dependence $I_P(q)$ does not possess any pronounced steps at $q < +18$. Hence, no ionization saturation is expected in accordance with the experiment. To resolve further details, we consider IDS charge-state resolved recoil energy spectra, Fig. U.12. The shapes are similar to argon in Fig. U.6, a, for which envelope has been assigned to incomplete explosion. Only the spectra of $q = 1..3$ span down to zero. For $q = 6..14$ the spectra show a peak shape, which exhibits a pronounced low energy cut-off, i.e., low energy ions are absent. The kinetic energies strongly depend on the charge state, e.g., $E_{max}^{q=1} \approx 2$ keV and $E_{max}^{q=12} \approx 12$ keV. Both of these features are typical for "shell-core" explosion as observed in argon clusters. This leads to the conclusion that recombination in silver is significantly higher than in argon at comparable conditions. Qualitatively this can be understood, when one considers the three body recombination rate, see Sec. 1.3.4. Compared to argon, silver has lower Wigner-Seitz radius, and hence, an initially higher ion density n_i. After ionization, electron densities n_e are higher as well. Additionally, Ag ions are heavier and thus expand slower. The more efficient screening of the laser field leads to lower electron temperatures T_e. Most likely, the combination of these factors causes the considered difference between silver and argon clusters.

To observe complete disintegration, we applied laser double pulses, as was done in [47,168–170]. Pump and probe are 130 fs long with peak intensitieas of $I_{Las} = 6.4 \cdot 10^{14}$ W/cm^2. The pump initiates the cluster expansion and the interaction with pre-expanded clusters is studied with a delayed probe. By varying the time delay τ between the pulses, we thus control the target ion density. We emphasize that no IDS is applied and the effect of the laser intensity averaging over the focal volume is present in spectra. Total ion yields as function of τ ($\overline{N} = 8500$ and 65000 atoms) are shown in Fig. U.13.

A strong pump-probe effect is observed. The yields at resonant and non-resonant conditions differ by more then factor of two. The optimal delay τ_{res} depends on the cluster size: for smaller clusters, $\tau_{res}^{8500} = 1.5$ ps, whereas $\tau_{res}^{65000} = 4.0$ ps for larger ones. The peak width is

cluster size dependent as well. For Ag_{65000} the peak width is more then doubled compared to Ag_{8500} on a signal level of 75% of maximum. This may be explained by the broader cluster size distribution, since the full-width half-maximum of log-normal distributions increases with increasing average.

Since no IDS spectra of complete cluster disintegration have been recorded, we cannot determine an average ion recoil energy. However, the information when the cluster achieves the resonance density allows us to make a rough estimate of the expansion velocity after the pump pulse. For that reason the nanoplasma is modelled as a uniformly charged sphere that expands under the action of Coulomb forces and achieves resonant ion density within τ_{res}. The corresponding final average ion kinetic energy is calculated. The results $E_{avg}^{8500} \approx$ 70 eV and $E_{avg}^{65000} \approx 40$ eV give an estimate of the average kinetic energy of the cluster core.

In Fig. U.14 ion spectra corresponding to pump-only (blue) and resonant pump-probe (orange) excitations are shown. For single pulses, the spectra span up to 8.5 keV. This value is more then two orders of magnitude higher then estimated E_{avg}^{8500} and E_{avg}^{65000}. This result suggests a "shell-core" disintegration scenario, similar to what is observed in argon clusters. For resonant absorption, the kinetic energies are even higher by more then an order of magnitude. Strong size effects are obtained: E_{max}^{8500}=82 keV is more then two times lower compared to E_{max}^{65000}=174 keV. Similar trends have been observed in rare gas clusters before [14, 88, 144, 145]. Most likely, at resonance larger clusters absorb more energy from the laser field, which leads to the emission of faster ions. However, when the ion density is beyond the resonance, electrons screen the cluster core. This is more effective in larger clusters, which results in a less efficient energy absorption. Additionally, the decrease of the ion density during the laser pulse is lower for larger clusters, which leads to better screening of cluster core. Hence, the opposite trend is observed in pump-probe when compared to single pulse excitation.

Figure U.14.: Recoil energy spectra of ions emitted from clusters exposed to single and double pulses. Pump and probe pulses are applied with optimal delays τ_{res}, see Fig. U.13. A strong dependence of ion recoil energy on average cluster size is observed.
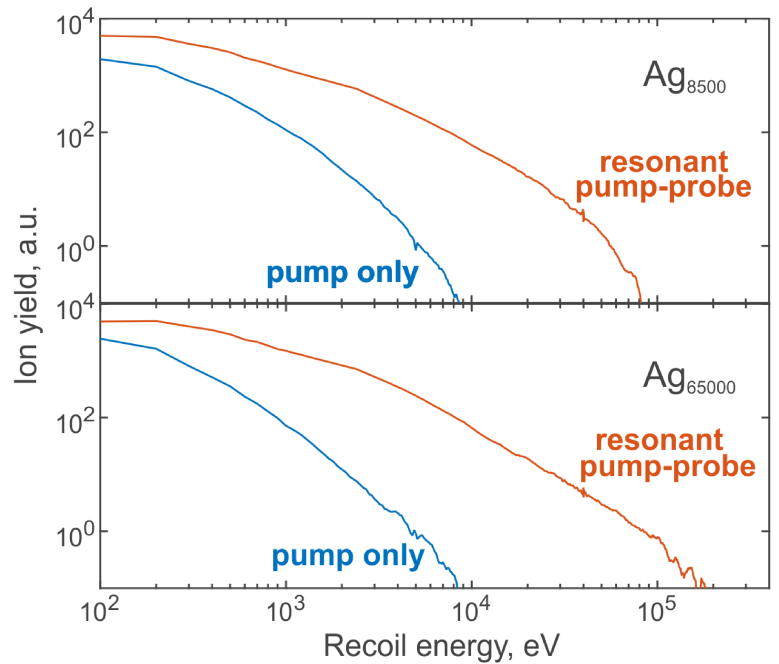

61

Figure U.15.: Charge-state resolved recoil energy spectra of ions from Ag_{8500} clusters. Blue dots represent data recorded with excitation by a pump laser pulse only, orange dots correspond to resonant excitation with double pulses. Single pulse spectra suggest that clusters undergo "shell-core" explosion, whereas the shapes of the pump-probe spectra corresponds to a "homogeneous" cluster expansion.
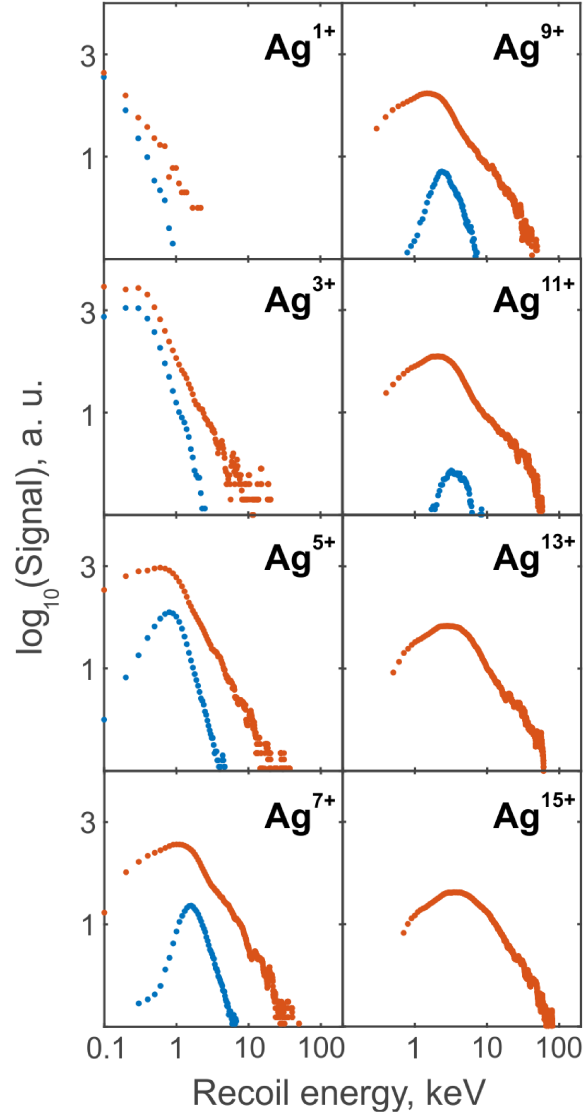
In Fig. U.15, we present charge resolved recoil energy spectra obtained with pump-only (blue) and resonant pump-probe (orange) pulses. When excited resonantly, higher ion yields are observed for all charge states. At the same q, more energetic ions are emitted at resonance. Higher charge states are achieved as well, e.g., $q = 13, 15$. The maximal observed charge state is $q = 20$. We note the qualitative difference in the shapes of the high-q spectra, e.g., $q = 5, 7, 9, 11$. When exposed to a single pulse only, the shape can be attributed to "shell-core" explosion. When excited resonantly, the pronounced low-energy cut-offs disappear. This is an indication that a complete cluster explosion occurs and recombination is frustrated.

Bibliography

[1] H.A. Haus. Mode-locking of lasers. *IEEE J. Sel. Top. Quantum Electron.*, 6:1173–1185, 2000.

[2] D.E. Spence, P.N. Kean, and W. Sibbett. 60-fsec pulse generation from a self-mode-locked Ti-Sapphire laser. *Opt. Lett.*, 16:42–44, 1991.

[3] P. Maine, D. Strickland, P. Bado, M. Pessot, and G. Mourou. Generation of ultrahigh peak power pulses by chirped pulse amplification. *J. Quant. Electr.*, 24:398, 1988.

[4] K.F. Renk. *Basics of Laser Physics*. Springer, Berlin Heidelberg, 2012.

[5] P. B. Corkum. Plasma perspective on strong field multiphoton ionization. *Phys. Rev. Lett.*, 71:1994–1997, 1993.

[6] B. Walker, B. Sheehy, L. F. DiMauro, P. Agostini, K. J. Schafer, and K. C. Kulander. Precision measurement of strong filed double ionization of helium. *Phys. Rev. Lett.*, 73:1227–30, 1994.

[7] M. Protopapas, C.H. Keitel, and P.L. Knight. Atomic physics with super-high intensity lasers. *Rep. Prog. Phys.*, 60:389–486, 1997.

[8] P. B. Corkum and F. Krausz. Attosecond science. *Nat. Phys.*, 3:381–387, 2007.

[9] Th. Brabec and F. Krausz. Intense few-cycle laser fields: Frontiers of nonlinear optics. *Rev. Mod. Phys.*, 72:545–592, 2000.

[10] F. Krausz and M. Ivanov. Attosecond physics. *Rev. Mod. Phys.*, 81:163–234, 2009.

[11] P.M. Paul, E.S. Toma, P. Breger, G. Mullot, F. Auge, P. Balcou, H.G. Muller, and P. Agostini. Observation of a train of attosecond pulses from high harmonic generation. *Science*, 292:1689–1692, 2001.

[12] T. Gaumnitz, A. Jain, Y. Pertot, M. Huppert, I. Jordan, F. Ardana-Lamas, and H.J. Wörner. Streaking of 43-attosecond soft-x-ray pulses generated by a passively cep-stable mid-infrared driver. *Opt. Express*, 25:27506–27518, 2017.

[13] H. Wang, Y. Xu, S. Ulonska, J.S. Robinson, P. Ranitovic, and R.A. Kaindl. Bright high-repetition-rate source of narrowband extreme-ultraviolet harmonics beyond 22 eV. *Nat. Commun.*, 6, 2015.

[14] T. Ditmire, R. A. Smith, J. W. G. Tisch, and M. H. R. Hutchinson. High Intensity Laser Absorption by Gases of Atomic Clusters. *Phys. Rev. Lett.*, 78:3121–4, 1997.

[15] M. Lezius, S. Dobosz, D. Normand, and M. Schmidt. Hot nanoplasmas from intense laser irradiation of argon clusters. *J. Phys. B*, 30:L251–8, 1997.

[16] T. Ditmire, T. Donnelly, A. M. Rubenchik, R. W. Falcone, and M. D. Perry. Interaction of intense laser pulses with atomic clusters. *Phys. Rev. A*, 53:3379–402, 1996.

[17] T. Ditmire, J.W.G. Tisch, E. Springate, M.B. Mason, N. Hay, R.A. Smith, I. Marangos, and M.M.R. Hutchinson. High energy ions produced in explosions of superheated atomic clusters. *Nature*, 386:54–56, 1997.

[18] Y. L. Shao, T. Ditmire, J. W. G. Tisch, E. Springate, J. P. Marangos, and M. H. R. Hutchinson. Multi-keV Elektron Generation in the Interaction of Intense Laser Pulses with Xe Clusters. *Phys. Rev. Lett.*, 77(16):3343–6, October 1996.

[19] T. Ditmire, T. Donelly, R.W. Falcone, and M.D. Perry. Strong X-ray emission from high-temperature plasmas produced by intense irradiation of clusters. *Phys. Rev. Lett.*, 75:3122–3125, 1995.

[20] T. Ditmire, J. Zweiback, V.P. Yanovsky, T.E. Cowan, G. Hays, and K.B. Wharton. Nuclear fusion from explosions of femtosecond laser-heated deuterium clusters. *Nature*, 398:489–491, 1999.

[21] U. Saalmann, C. Siedschlag, and J. M. Rost. Mechanisms of cluster ionization in strong laser pulses. *J. Phys. B*, 39:R39, 2006.

[22] Th. Fennel, K.-H. Meiwes-Broer, J. Tiggesbäumker, P.-G. Reinhard, P. M. Dinh, and E. Suraud. Laser-driven nonlinear cluster dynamics. *Rev. Mod. Phys.*, 82:1793–1842, 2010.

[23] L. Englert, M. Wollenhaupt, L. Haag, C. Sarpe-Tudoran, B. Rethfeld, and T. Baumert. Material processing of dielectrics with temporally asymmetric shaped femtosecond laser pulses on the nanometer scale. *Appl. Phys. A*, 92:749, 2008.

[24] T. Popmintchev, M.-C. Chen, D. Popmintchev, P. Arpin, S. Brown, S. Ališauskas, G. Andriukaitis, T. Balčiunas, O. D. Mücke, A. Pugzlys, A. Baltuška, B. Shim, S. E. Schrauth, A. Gaeta, C. Hernández-García, L. Plaja, A. Becker, A. Jaron-Becker, M. M. Murnane, and H. C. Kapteyn. Bright Coherent Ultrahigh Harmonics in the keV X-ray Regime from Mid-Infrared Femtosecond Lasers. *Science*, 336:1287–1291, 2012.

[25] K.W.D. Ledingham, P.R. Bolton, N. Shikazono, and C.M.C. Ma. Towards Laser Driven Hadron Cancer Radiotherapy: A Review of Progress. *Appl. Sci.-Basel*, 4:402–443, 2014.

[26] J. Passig, S. Zherebtsov, R. Irsig, M. Arbeiter, Ch. Peltz, S. Goede, S. Skruszewicz, K.H. Meiwes-Broer, J. Tiggesbaeumker, M.F. Kling, and Th. Fennel. Nanoplasmonic electron acceleration by attosecond-controlled forward rescattering in silver clusters. *Nat. Comm.*, 8, 2017.

[27] B. Schuette, F. Campi, M. Arbeiter, Th. Fennel, M. J. J. Vrakking, and A. Rouzee. Tracing Electron-Ion Recombination in Nanoplasmas Produced by Extreme-Ultraviolet Irradiation of Rare-Gas Clusters. *Phys. Rev. Lett.*, 112:253401, 2014.

[28] J.J. Thomson. Rays of positive electricity. *Phil. Mag.*, 6:752–767, 1911.

[29] Th. Fennel, L. Ramunno, and Th. Brabec. Highly Charged Ions from Laser-Cluster Interactions: Local-Field-Enhanced Impact Ionization and Frustrated Electron-Ion Recombination. *Phys. Rev. Lett.*, 99:233401, 2007.

[30] E. Skopalová, Y. C. El-Taha, M. Hohenberger A. Zaïr, E. Springate, J. W. G. Tisch,

R. A. Smith, and J. P. Marangos. Pulse-Length Dependence of the Anisotropy of Laser-Driven Cluster Explosions: Transition to the Impulsive Regime for Pulses Approaching the Few-Cycle Limit. *Phys. Rev. Lett.*, 104:203401, 2010.

[31] P. Wang, A. M. Sayler, K. D. Carnes, B. D. Esry, and I. Ben-Itzhak. Disentangling the volume effect through intensity-difference spectra: application to laser-induced dissociation of H_2^+. *Opt. Lett.*, 30:664–666, 2005.

[32] E. M. Snyder, S. A. Buzza, and A. W. Castleman Jr. Intense Field-Matter Interactions: Multiple Ionization of Clusters. *Phys. Rev Lett.*, 77:3347–50, 1996.

[33] M. Damgarten, M. Dörr, U. Eichmann, E. Lenz, and W. Sandner. Relativistic laser-field-drift suppression of nonsequential multiple ionization. *Phys. Rev. A*, 64:061402, 2001.

[34] Z.Q. Lin, J. Zhang, Y.J. Li, L.M. Chen, T.Z. Lu, H. Teng, B.Y. Man, and L.Z. Zhao. Measurements of laser absorption and ion energy in femtosecond laser-cluster interaction. *Chin. Phys. Lett.*, 18:211, 2001.

[35] E. Miura, Hiroshi Honda, Keisuke Katsura, E. Takahashi, and K. Kondo1. Enhancement of X-ray emission from a cooled Kr gas jet irradiated by an ultrashort KrF laser pulse. *Jap. J. Appl. Phys.*, 40:7067–7071, 2001.

[36] K. Yamakawa, Y. Akahane, Y. Fukuda, M. Aoyama, N. Inoue, H. Ueda, and T. Utsumi. Many-electron dynamics of a Xe atom in strong and superstrong laser fields. *Phys. Rev. Lett.*, 92:123001, 2004.

[37] L. Köller, M. Schumacher, J. Köhn, S. Teuber, J. Tiggesbäumker, and K.-H. Meiwes-Broer. Plasmon-Enhanced Multi-Ionization of Small Metal Clusters in Strong Femtosecond Laser Fields. *Phys. Rev. Lett.*, 82:3783–6, 1999.

[38] M. Schumacher, S. Teuber, L. Köller, J. Köhn, T. Tiggesbäumker, and K.-H. Meiwes-Broer. Clusters in Strong Laser Fields: Comparison between Carbon, Platinum, and Lead Clusters. *Eur. Phys. J. D*, 9:411–414, 1999.

[39] M.A. Lebeault, J. Vialln, J. Chevaleyre, C. Ellert, D.Normand, M.Schmidt, O. Sublemontier, C. Guet, and B. Huber. Resonant coupling of small size-controlled lead clusters with an intense laser field. *Eur. Phys. J. D.*, 20:233–242, 2002.

[40] P. Radcliffe, T. Döppner, M. Schumacher, S. Teuber, J. Tiggesbäumker, and K.H. Meiwes-Broer. Generation of Highly Charged and Energetic Ions From the Interaction of Strong Laser Pulses with Coinage Metal Clusters. *Contrib. Plas. Phys.*, 45:424, 2005.

[41] J.V. Ford, Q. Zhong, L. Poth, and A.W. Castleman Jr. Femtosecond laser interactions with methyl iodide clusters. I. Coulomb explosion at 795 nm. *J. Chem. Phys.*, 110:6257–6267, 1999.

[42] V. Kumarappan, M. Krishnamurthy, and D. Mathur. Explosions of water clusters in intense laser fields. *Phys. Rev. A*, 67:063207, 2003.

[43] V. Kumarappan, M. Krishnamurthy, and D. Mathur. Two-dimensional effects in the hydrodynamic expansion of xenon clusters under intense laser irradiation. *Phys. Rev.*

A, 66:33203, 2002.

[44] E. Springate, S. A. Aseyev, S. Zamith, and M. J. J. Vrakking. Electron kinetic energy measurements from laser irradiation of clusters. *Phys. Rev. A*, 68:053201, 2003.

[45] V. Kumarappan, M. Krishnamurthy, and D. Mathur. Asymmetric emission of high-energy electrons in the two-dimensional hydrodynamic expansion of large xenon clusters irradiated by intense laser fields. *Phys. Rev. A*, 67:043204, 2003.

[46] Th. Fennel, T. Döppner, J. Passig, Ch. Schaal, J. Tiggesbäumker, and K.-H. Meiwes-Broer. Plasmon-Enhanced Electron Acceleration in Intense Laser Metal-Cluster Interactions. *Phys. Rev. Lett.*, 98:143401, 2007.

[47] J Passig, R Irsig, N X Truong, Th Fennel, J Tiggesbäumker, and K H Meiwes-Broer. Nanoplasmonic electron acceleration in silver clusters studied by angular-resolved electron spectroscopy. *New J. Phys.*, 14:085020, 2012.

[48] S. Zherebtsov, Th. Fennel, J. Plenge, E. Antonsson, I. Znakovskaya, A. Wirth, O. Herrwerth, F. Suszmann, Ch. Peltz, I. Ahmad, S. A. Trushin, V. Pervak, S. Karsch, M. J. J. Vrakking, B. Langer, Ch. Graf, M. I. Stockman, F. Krausz, E. Ruhl, and M. F. Kling. Controlled near-field enhanced electron acceleration from dielectric nanospheres with intense few-cycle laser fields. *Nature Phys.*, 7:656, 2011.

[49] J. Larsson and A. Sjögren. Evaluation of laser-irradiated Ar clusters as a source for time-resolved x-ray studies. *Rev. Sci. Instr.*, 70:2253–2256, 1999.

[50] K. Kondo, M. Mori, and T. Shiraishi. X-ray generation from fs laser heated Xe clusters. *Appl. Surf. Sci.*, 197:138–144, 2002.

[51] R.C. Issac, G. Vieux, B. Ersfeld, E. Brunetti, S.P. Jamison, J. Gallacher, D. Clark, and D.A. Jaroszynski. Ultra hard x–rays from krypton clusters heated by intense laser fields. *Phys. Plas.*, 11:3491–3496, 2004.

[52] A. McPherson, T.S. Luk, B.D. Thompson, K. Boyer, and C.K. Rhodes. Multiphoton-induced X-ray emission and amplification from clusters. *Appl. Phys. B*, 57:337–348, 1993.

[53] A. McPherson, B.D. Thompson, A.B. Borisov, K. Boyer, and C.K. Rhodes. Multiphoton-induced X-ray emission at 4-5 keV from Xe atoms with multiple core vacancies. *Nature*, 370:631–633, 1994.

[54] I. Yu. Skobelev, A. Ya. Faenov, A. I. Magunov, T. A. Pikuz, A. S. Boldarev, V. A. Gasilov, J. Abdallach, G. C. Junkel-Vives, T. Auguste, S. Dobosz, P. D'Oliveira, S. Hulin, P. Monot, F. Blasco, F. Dorchies, T. Caillaud, C. Bonte, C. Stenz, F. Salin, P. A. Loboda, I. A. Litvinenko, V. V. Popova, G. V. Baidin, and B. Yu. Sharkov. X-ray spectroscopy diagnostic of a plasma produced by femtosecond laser pulses irradiating a cluster target. *J. Exp. Theor. Phys.*, 94:966–976, 2002.

[55] S. Dobosz, M. Lezius, M. Schmidt, P. Meynadier, M. Perdrix, D. Normand, J.-P. Rozet, and D. Vernhet. Absolute keV photon yields from ultrashort laser-field-induced hot nanoplasmas. *Phys. Rev. A*, 56:R2526–R2529, 1997.

[56] J.P. Rozet, M. Cornille, S. Dobosz, J. Dubau, J.C. Gauthier, S. Jacquemot, E. Lamour,

M. Lezius, D. Normand, M. Schmidt, and D. Vernhet. State selective measurements of HCl produced by strong ultrashort laser-clusters interaction. *Phys. Scr.*, T92:113–118, 2001.

[57] E. Lamour, C. Prigent, J.P. Rozet, and D. Vernhet. Physical parameter dependence of the X-ray generation in intense laser-cluster interaction. *Nucl. Instr. Meth. B*, 235:408–413, 2005.

[58] E. Lamour, C. Prigent, J.P. Rozet, and D Vernhet. X-ray production in short laser pulse interaction with rare gas clusters. *J. Phys. Conf. Series*, 88:012035, 2007.

[59] Ch. Prigent, C. Deiss, E. Lamour, J.-P. Rozet, D. Vernhet, and J. Burgdoerfer. Effect of pulse duration on the x-ray emission from Ar clusters in intense laser fields. *Phys. Rev. A*, 78:053201, 2008.

[60] B. A. M. Hansson, O. Hemberg, H. M. Hertz, M. Berglund, H.-J. Choi, B. Jacobsson, E. Janin, S. Mosesson, L. Rymell, J. Thoresen, and M. Wilner. Characterization of a liquid-xenon-jet laser-plasma extreme-ultraviolet source. *Rev. Sci Instr.*, 75:2122, 2004.

[61] Y. Fukuda, A. Ya. Faenov, T. Pikuz, M. Kando, H. Kotaki, I. Daito, J. Ma, L. M. Chen, T. Homma, K. Kawase, T. Kameshima, T. Kawachi, H. Daido, T. Kimura, T. Tajima, Y. Kato, and S. V. Bulanov. Soft x-ray source for nanostructure imaging using femtosecond-laser-irradiated clusters. *Appl Phys. Lett.*, 92:121110, 2008.

[62] Ch. Schaal. Rostock, 2013. PhD thesis.

[63] W.A. de Heer. The physics of simple metal clusters: Experimental aspects and simple models. *Rev. Mod. Phys.*, 65:611–676, 1993.

[64] G. Scoles. *Atomic and molecular beam methods Vol. I.* Oxford University Press, New York, 1988.

[65] O. F. Hagena and W. Obert. Cluster formation in expanding supersonic jets: Effect of pressure, temperature, nozzle size, and test gas. *J. Chem. Phys.*, 56:1793–1802, 1972.

[66] O.F. Hagena. Nucleation and growth of clusters in expanding nozzle flows. *Surf. Sci.*, 106:101–116, 1981.

[67] O.F. Hagena. Condensation in free jets: Comparision of rare gases and metals. *Z. Phys. D*, 4:291–299, 1987.

[68] D. Pentlehner, R. Riechers, B. Dick, A. Slenczka, U. Even, N. Lavie, R. Brown, and K. Luria. Rapidly pulsed helium droplet source. *Rev. Sci. Instr.*, 80:043302, 2009.

[69] H. Haberland, M. Karrais, M. Mall, and Y. Thurner. Thin-films from energetic cluster impact – a feasibility study. *J. Vac. Sci. Technol. A*, 10:3266, 1992.

[70] H. R. Siekmann, Ch. Lüder, J. Faehrmann, H. O. Lutz, and K.-H. Meiwes-Broer. The pulsed arc cluster ion source (PACIS). *Z. Phys. D*, 20:417–20, 1991.

[71] C.-Y. Cha, G. Ganteför, and W. Eberhardt. New experimental setup for photoelectron spectroscopy on cluster anions. *Rev. Sci. Instr.*, 63:5661–6, 1992.

[72] R.-P. Methling, V. Senz, E.-D. Klinkenberg, Th. Diederich, J. Tiggesbäumker,

G. Holzhüter, J. Bansmann, and K.-H. Meiwes-Broer. Magnetic studies on mass-selected iron particles. *Eur. Phys. J. D*, 16:173–176, 2001.

[73] A. Kleibert, J. Passig, K.-H. Meiwes-Broer, M. Getzlaff, and J. Bansmann. Structure and magnetic moments of mass-filtered deposited nanoparticles. *J. Appl. Phys.*, 101:114318, 2007.

[74] E.A. Rohlfing. Optical-Emission Studies of Atomic, Molecular, and Particulate Carbon Produced from a Laser Vaporization Cluster Source. *J. Chem. Phys.*, 89:6103–6112, 1988.

[75] P. Milani and W. A. deHeer. Improved pulsed laser vaporization source for production of intense beams of neutral and ionized clusters. *Rev. Sci. Instr.*, 61:1835–1838, 1990.

[76] S. Goyal, D.L. Schutt, and G. Scoles. Vibrational spectroscopy of sulfur hexafluoride attached to helium clusters. *Phys. Rev. Lett.*, 69:933–936, 1992.

[77] A. Bartelt, J.D. Close, F. Federmann, N. Quaas, and J.-P. Toennies. Cold metal clusters: Helium droplets as a nanoscale cryostat. *Phys. Rev. Lett.*, 77:3525–3528, 1996.

[78] J. Tiggesbäumker and F. Stienkemeier. Formation and properties of metal clusters isolated in helium droplets. *Phys. Chem. Chem. Phys.*, 9:4748 – 4770, 2007.

[79] D. Rupp, L. Flückiger, M. Adolph, T. Gorkhover, M. Krikunova, J.P. Müller, M. Müller, T. Oelze, Y. Ovcharenko, B. Röben, M. Sauppe, S. Schorb, D. Wolter, R. Mitzner, M. Wöstmann, S. Roling, M. Harmand, R. Treusch, M. Arbeiter, Th. Fennel, Ch. Bostedt, and Th. Möller. Recombination-enhanced surface expansion of clusters in intense soft x-ray laser pulses. *Phys. Rev. Lett.*, 117:153401, 2016.

[80] J. Passig. Rostock, 2012. PhD thesis.

[81] P. Kruit and F.H. Read. Magnetic field paralleliser for 2π electron-spectrometer and electron-image magnifier. *J. Phys. E.*, 16:313, 1983.

[82] G. Ganteför, K.-H. Meiwes-Broer, and H.O. Lutz. Photodetachment Spectroscopy of Cold Aluminium Cluster Anions. *Phys. Rev. A*, 37:2716, 1988.

[83] D.W. Arnold, S.E. Bradford, and T.N. Kitsopoulosand D.M. Neumark. Vibrationally resolved spectra of C_2-C_{11} by anion photoelectron spectroscopy. *J. Chem. Phys.*, 95:8753, 1991.

[84] A.T.J.B. Eppink and D.H. Parker. Velocity map imaging of ions and electrons using electrostatic lenses: Application in photoelectron and photofragment ion imaging of molecular oxygen. *Rev. Sci. Instr.*, 68:3477–3484, 1997.

[85] S. Skruszewicz, J. Passig, A. Przystawik, N.X. Truong, M. Köther, J. Tiggesbäumker, and K.-H. Meiwes-Broer. A new design for imaging of fast energetic electrons. *Int. J Mass Spectr.*, 365-366:338, 2014.

[86] R. Irsig. Rostock, 2017. PhD thesis.

[87] S. Fuchs, C. Roedel, M. Krebs, S. Haedrich, J. Bierbach, A. E. Paz, S. Kuschel, M. Wuensche, V. Hilbert, U. Zastrau, E. Foerster, J. Limpert, and G. G. Paulus. Sensitivity calibration of an imaging extreme ultraviolet spectrometer-detector system

for determining the efficiency of broadband extreme ultraviolet sources. *Rev. Sci. Instr.*, 84:023101, 2013.

[88] M. Lezius, S. Dobosz, D. Normand, and M. Schmidt. Explosion Dynamics of Rare Gas Clusters in Strong Laser Fields. *Phys. Rev. Lett.*, 80:261–4, 1998.

[89] M. Lezius. A B-TOF mass spectrometer for the analysis of ions with extreme high start-up energies. *J. Mass. Spectr.*, 37:305, 2002.

[90] J.J. Thomson. *Phil. Mag.*, 13:561, 1907.

[91] M. Hirokane, S. Shimizu, M. Hashida, S. Okada, S. Okihara, F. Sato, T. Iida, and S. Sakabe. Energy distributions of ions emitted from argon clusters Coulomb-exploded by intense femtosecond laser pulses. *Phys. Rev. Lett.*, 69:063201, 2004.

[92] R. Rajeev, K. P. M. Rishad, T. Madhu Trivikram, V. Narayanan, and M. Krishnamurthy. A thomson parabola ion imaging spectrometer designed to probe relativistic intensity ionization dynamics of nanoclusters. *Rev. Sci. Instrum.*, 82(8):083303, 2011.

[93] T. Döppner and S. Teuber and Th. Diederich and Th. Fennel and P. Radcliffe and J. Tiggesbäumker and K.H. Meiwes-Broer. Dynamics of Free and Embedded Lead Clusters in Intense Laser Fields. *Eur. Phys. J. D.*, 24:157–160, 2003.

[94] G.S. Voronov and N.B. Delone. Ionization of xenon aatom by electric field of ruby laser emission. *JETP Lett.*, 1:66–68, 1965.

[95] L. V. Keldysh. Ionization in the field of a strong electromagnetic wave. *Sov. Phys. JETP*, 20:1307–14, 1965.

[96] M.J. DeWitt and R.J. Levis. Calculating the keldysh adiabaticity parameter for atomic, diatomic, and polyatomic molecules. *J. Chem. Phys.*, 108:7739–7742, 1998.

[97] M. V. Ammosov, N. B. Delone, and V. P. Kraĭnov. Tunnel ionization of complex atoms and of atomic ions in an alternating electromagnetic field. *Sov. Phys. JETP*, 64:1191–4, 1986.

[98] N.B. Delone and V.P. Krainov. Tunneling and barrier-suppresion ionization of atoms and ions in a laser radiation field. *Phys. Usp.*, 41:469–485, 1998.

[99] S. Augst, D. Strickland, D. D. Meyerhofer, S. L. Chin, and J. H. Eberly. Tunneling Ionization of Noble Gases in a High-Intensity Laser Field. *Phys. Rev. Lett.*, 63:2212–5, 1989.

[100] A. Kramida, Yu. Ralchenko, J. Reader, and NIST ASD Team. NIST Atomic Spectra Database (ver. 5.3), National Institute of Standards and Technology, Gaithersburg, MD., 2015.

[101] I. Last and J. Jortner. Quasiresonance ionization of large multicharged clusters in a strong laser field. *Phys. Rev. A*, 60:2215–2221, 1999.

[102] T. Döppner, J.P. Müller, A. Przystawik, S. Göde, J. Tiggesbäumker, K.-H. Meiwes-Broer, C. Varin, L. Ramunno, T. Brabec, and T. Fennel. Steplike intensity threshold behavior of extreme ionization in laser-driven Xe clusters. *Phys. Rev. Lett.*, 105:053401, 2010.

[103] B. Schuette, M. Arbeiter, A. Mermillod-Blondin, M.J.J. Vrakking, A. Rouzee, and Th. Fennel. Ionization Avalanching in Clusters Ignited by Extreme-Ultraviolet Driven Seed Electrons. *Phys. Rev. Lett.*, 116:033001, 2016.

[104] G. Mie. Beiträge zur Optik trüber Medien, speziell kolloidaler Metalllösungen. *Ann. Phys.*, 25:377–445, 1908.

[105] W. Ekardt. Work function of small metal particles: Self consistent spherical jellium-background model. *Phys. Rev. B*, 29:1558–1564, 1984.

[106] T. Döppner, Th. Fennel, Th. Diederich, J. Tiggesbäumker, and K.-H. Meiwes-Broer. Controlling the Coulomb Explosion of Silver Clusters by Femtosecond Dual-Pulse Laser Excitation. *Phys. Rev. Lett.*, 94:013401, 2005.

[107] E. Springate, N. Hay, J. W. G. Tisch, M. B. Mason, T. Ditmire, J. P. Marangos, and M. H. R. Hutchinson. Enhanced explosion of atomic clusters irradiated by a sequence of two high-intensity laser pulses. *Phys. Rev. A*, 61:44101–4, 2000.

[108] V. Kumarappan, M. Krishnamurthy, and D. Mathur. Asymmetric High-Energy Ion Emission from Argon Clusters in Intense Laser Fields. *Phys. Rev. Lett.*, 87:085005, 2001.

[109] Th. Fennel, K.-H. Meiwes-Broer, and G.F. Bertsch. Ionization dynamics of simple metal clusters in intense laser fields by the Thomas-Fermi-Vlasov method. *Eur. Phys. J. D*, 29:367–378, 2004.

[110] Ch. Jungreuthmayer, M. Geissler, J. Zanghellini, and Th. Brabec. Microscopic Analysis of Large-Cluster Explosion in Intense Laser Fields. *Phys. Rev. Lett.*, 92:133401, 2004.

[111] B.N. Breizman, A.V. Arefiev, and M.V. Fomytskyi. Nonlinear physics of laser-irradiated microclusters. *Phys. Plas.*, 12:056706, 2005.

[112] D. Mathur, F. A. Rajgara, A. R. Holkundkar, and N. K. Gupta. Strong-field ionization and coulomb explosion of argon clusters by few-cycle laser pulses. *Phys. Rev. A*, 82:025201, 2010.

[113] D. Mathur and F. A. Rajgara. Communication: Ionization and Coulomb explosion of xenon clusters by intense, few-cycle laser pulses. *J. Chem. Phys.*, 133:061101, 2010.

[114] D. Mathur and F.A. Rajgara. Dynamics of atomic clusters in intense optical fields of ultrashort duration. *J. Chem. Sci.*, 124:75–81, 2012.

[115] G. Mishra and N. K. Gupta. Molecular dynamic studies on anisotropic explosion of laser irradiated xe cluster. *Phys. Plasmas*, 19:093107, 2012.

[116] B. Schuette, M.J.J. Vrakking, and A. Rouzee. Tracing transient charges in expanding clusters. *Phys. Rev. A*, 95:063417, 2017.

[117] A. Galeev and R. Sudan. *Osnovy fiziki plazmy, tom 1*. Energoatomizdat, Moskva, 1983, in russian only.

[118] B. Schuette, M. Arbeiter, Th. Fennel, M. J. J. Vrakking, and A. Rouzée. Rare-gas clusters in intense extreme-ultraviolet pulses from a high-order harmonic source. *Phys.*

Rev. Lett., 112:073003, 2014.

[119] B. Schuette, M. Arbeiter, Th. Fennel, G. Jabbari, A.I. Kuleff, M. J. J. Vrakking, and A. Rouzée. Observation of correlated electronic decay in expanding clusters triggered by near-infrared fields. *Nature Comm.*, 6, 2015.

[120] B. Schuette, J. Lahl, T. Oelze, M. Krikunova, M.J.J. Vrakking, and A. Rouzee. Autoionization following nanoplasma formation in atomic and molecular clusters. *Eur. Phys. J. D*, 70:115, 2016.

[121] R. Rajeev, T. Madhu Trivikram, K. P. M. Rishad, V. Narayanan, E. Krishnakumar, and M. Krishnamurthy. A compact laser-driven plasma accelerator for megaelectronvolt-energy neutral atoms. *Nature Phys.*, 9:185–190, 2013.

[122] R. Rajeev, T. Madhu Trivikram, K. P. M. Rishad, and M. Kishnamurthy. Anisotropic emission of neutral atoms: evidence of an anisotropic Rydberg sheath in nanoplasma. *New J. Phys.*, 17:023033, 2015.

[123] R. Rajeev, Malay Dalui, T. Madhu Trivikram, K. P. M. Rishad, and M. Krishnamurthy. Anisotropic negative-ion emission from cluster nanoplasmas. *Phys. Rev. A*, 91:063403, 2015.

[124] H.M. Milchberg, S.J. McNaught, and E. Parra. Plasma hydrodynamics of the intense laser-cluster interaction. *Phys. Rev. E*, 64:056402, 2001.

[125] C. Rose-Petruck, K.J. Schäfer, K.R. Wilson, and C.P.J. Barty. Ultrafast electron dynamics and inner-shell ionization in laser driven clusters. *Phys. Rev. A*, 55:1182–1190, 1997.

[126] T. Ditmire, E. Springate, J.W.G. Tisch, Y.L. Shao, M.B. Mason, N. Hay, J.P. Marangos, and M.H.R. Hutchinson. Explosion of atomic clusters heated by high-intensity femtosecond laser pulses. *Phys. Rev. A*, 57:369, 1998.

[127] I. Last and J. Jortner. Theoretical study of multielectron dissociative ionization of diatomic molecules and clusters in a strong laser field. *Phys. Rev. A*, 58:3826–3835, 1998.

[128] I. Last and J. Jortner. Dynamics of the Coulomb explosion of large clusters in a strong laser field. *Phys. Rev. A*, 62:013201, 2000.

[129] K Ishikawa and T. Blenski. Explosion dynamics of rare-gas clusters in an intense laser field. *Phys. Rev. A*, 62:63204–63400, 2000.

[130] Ch. Siedschlag and J.M. Rost. Electron Release of Rare-Gas Atomic Clusters under an Intense Laser Pulse. *Phys. Rev. Lett.*, 89:173401, 2002.

[131] Ch. Siedschlag and J. M. Rost. Small Rare-Gas Clusters in Soft X-Ray Pulses. *Phys. Rev. Lett.*, 93:043402, 2004.

[132] E. S. Toma and H. G. Muller. Laser disintegration of Van der Waals clusters of carbon-containing molecules. *Phys. Rev. A*, 66:013204, 2002.

[133] U. Saalmann and J.-M. Rost. Ionization of Clusters in Intense Laser Pulses through Collective Electron Dynamics. *Phys. Rev. Lett.*, 91:223401, 2003.

[134] D. Bauer. Small rare gas clusters in laser fields: ionization and absorption at long and short laser wavelengths. *J. Phys. B*, 37:3085–3101, 2004.

[135] Ch. Jungreuthmayer, L. Ramunno, J. Zanghellini, and Th. Brabec. Intense VUV laser cluster interaction in the strong coupling regime. *J. Phys. B.*, 38:3029, 2005.

[136] Wolfgang Lotz. Electron-Impact Ionization Cross-Sections and Ionization Rate Coefficients for Atoms and Ions from Hydrogen to Calcium. *Z. Phys.*, 216:241–7, 1968.

[137] E. Ackad, N. Bigaouette, and L. Ramunno. Augmented collisional ionization via excited states in XUV cluster interactions. *J. Phys. B*, 44:165102, 2011.

[138] U. Saalmann and J. M. Rost. Electron dynamics in strong laser pulse illumination of large rare gas clusters. *Eur. Phys. J. D*, 36:159, 2005.

[139] M Krishnamurthy, J Jha, D Mathur, C Jungreuthmayer, L Ramunno, J Zanghellini, and T Brabec. Ion charge state distribution in the laser-induced Coulomb explosion of argon clusters. *J. Phys. B*, 39:625–632, 2006.

[140] M. Kundu and D. Bauer. Nonlinear Resonance Absorption in the Laser-Cluster Interaction. *Phys. Rev. Lett.*, 96:123401, 2006.

[141] G. M. Petrov and J. Davis. Interaction of intense ultrashort pulse lasers with clusters. *Phys. Plas.*, 15:056705, 2008.

[142] Ch. Peltz. Rostock. PhD thesis.

[143] Md.R. Islam, U. Saalmann, and J. M. Rost. Kinetic energy of ions after Coulomb explosion of clusters induced by an intense laser pulse. *Phys. Rev. A*, 73:041201, 2006.

[144] S. Sakabe, S. Shimizu, M. Hashida, F. Sato, T. Tsuyukushi, K. Nishihara, S. Okihara, T. Kagawa, Y. Izawa, K. Imasaki, and T. Iida. Generation of high-energy protons from the Coulomb explosion of hydrogen clusters by intense femtosecond laser pulses. *Phys. Rev. A*, 69:023203, 2004.

[145] M. Krishnamurthy, D. Mathur, and V. Kumarappan. Anisotropic charge-flipping acceleration of highly charged ions from clusters in strong optical fields. *Phys. Rev. A*, 69:033202, 2004.

[146] M. Almassarani. Rostock, 2016. Master thesis.

[147] M. Arndt. Greifswald, 2011. PhD thesis.

[148] H. Hartmann, V. N. Popok, I. Barke, V. von Oeynhausen, and K.-H. Meiwes-Broer. Design and capabilities of an experimental setup based on magnetron sputtering for formation and deposition of size-selected metal clusters on ultra-clean surfaces. *Rev. Sci. Instr.*, 83:073304, 2012.

[149] M. A. Walker, P. Hansch, and L. D. Van Woerkom. Intensity-resolved multiphoton ionization: Circumventing spatial averaging. *Phys. Rev. A*, 57:701–704, 1998.

[150] W.A. Bryan, S.L. Stebbings, J. McKenna, E.M.L. English, M. Suresh, J. Wood, B. Srigengan, I.C.E. Turcu, J.M. Smith, E.J. Divall, C.J. Hooker, A.J. Langley, J.L. Collier, I.D. Williams, and W.R. Newell. Atomic excitation during recollision-free

ultrafast multi-electron tunnel ionization. *Nature Phys.*, 2:379 – 383, 2006.

[151] S. G. Sayres, M. W. Ross, and A. W. Castleman. Influence of clustering and molecular orbital shapes on the ionization enhancement in ammonia. *Phys. Chem. Chem. Phys.*, 13:12231–12239, 2011.

[152] M.W. Ross and A. W. Castleman, Jr. Femtosecond ionization and Coulomb explosion of small transition metal carbide clusters. *Chem. Phys. Lett.*, 547:13–20, 2012.

[153] M.W. Ross and A. W. Castleman, Jr. Influence of Group 10 Metals on the Growth and Subsequent Coulomb Explosion of Small Silicon Clusters under Strong Light Pulses. *ChemPhysChem*, 14:771–776, 2013.

[154] M. M. Seibert, T. Ekeberg, F. R. N. C. Maia, M. Svenda, J. Andreasson, O. Joensson, D. Odic, B. Iwan, A. Rocker, D. Westphal, M. Hantke, D. P. DePonte, A. Barty, J. Schulz, L. Gumprecht, N. Coppola, A. Aquila, M. Liang, Th. A. White, A. Martin, C. Caleman, S. Stern, C. Abergel, V. Seltzer, J.-M. Claverie, Ch. Bostedt, J. D. Bozek, S. Boutet, A. A. Miahnahri, M. Messerschmidt, J. Krzywinski, G. Williams, K. O. Hodgson, M. J. Bogan, C. Y. Hampton, R. G. Sierra, D. Starodub, I. Andersson, S. Bajt, M. Barthelmess, J. C. H. Spence, P. Fromme, U. Weierstall, R. Kirian, M. Hunter, R. B. Doak, S. Marchesini, S. P. Hau-Riege, M. Frank, R. L. Shoeman, L. Lomb, S. W. Epp, R. Hartmann, D. Rolles, A. Rudenko, C. Schmidt, L. Foucar, N. Kimmel, P. Holl, B. Rudek, B. Erk, A. Hoemke, Ch. Reich, D. Pietschner, G. Weidenspointner, L. Strueder, G. Hauser, H. Gorke, J. Ullrich, I. Schlichting, S. Herrmann, G. Schaller, F. Schopper, H. Soltau, K.-U. Kuehnel, R. Andritschke, C.-D. Schroeter, F. Krasniqi, M. Bott, S. Schorb, D. Rupp, M. Adolph, T. Gorkhover, H. Hirsemann, G. Potdevin, H. Graafsma, B. Nilsson, H. N. Chapman, and J. Hajdu. Single mimivirus particles intercepted and imaged with an X-ray laser. *Nature*, 470:78–U86, 2011.

[155] I. Barke, H. Hartmann, D. Rupp, L. Flückiger, M. Sauppe, M. Adolph, S. Schorb, Ch. Bostedt, R. Treusch, Ch. Peltz, S. Bartling, Th. Fennel, K.-H. Meiwes-Broer, and Th. Möller. The 3D-architecture of individual free silver nanoparticles captured by X-ray scattering. *Nature Comm.*, 6:6187, 2015.

[156] D. Rupp, L. Flückiger, M. Adolph, T. Gorkhover, M. Krikunova, J.P. Müller, M. Müller, T. Oelze, Y. Ovcharenko, B. Röben, M. Sauppe, S. Schorb, D. Wolter, R. Mitzner, M. Wöstmann, S. Roling, M. Harmand, R. Treusch, M. Arbeiter, Th. Fennel, Ch. Bostedt, and Th. Möller. Recombination-enhanced surface expansion of clusters in intense soft x-ray laser pulses. *Phys. Rev. Lett.*, 117:153401, 2016.

[157] T. Gorkhover, S. Schorb, R. Coffee, M. Adolph, L. Foucar, D. Rupp, A. Aquila, J. D. Bozek, S. W. Epp, B. Erk, L. Gumprecht, L. Holmegaard, A. Hartmann, R. Hartmann, G. Hauser, P. Holl, A. Hoemke, P. Johnsson, N. Kimmel, K.-U. Kuehnel, M. Messerschmidt, C. Reich, A. Rouzee, B. Rudek, C. Schmidt, J. Schulz, H. Soltau, S. Stern, G. Weidenspointner, B. White, J. Kuepper, L. Strueder, I. Schlichting, J. Ullrich, D. Rolles, A. Rudenko, Th. Moeller, and C. Bostedt. Femtosecond and nanometre visualization of structural dynamics in superheated nanoparticles. *Nat. Photonics*, 10:93, 2016.

[158] A. Höll, Th. Bornath, L. Cao, T. Döppner, S. Düsterer, E. Förster, C. Fortmanna, S. H.

Glenzer, G. Gregori, T. Laarmann, K.-H. Meiwes-Broer, A. Przystawik, P. Radcliffe, R. Redmer, H. Reinholz, G. Röpke, R. Thiele, J. Tiggesbäumker, S. Toleikis, N.X. Truong, T. Tschentscher, I. Uschmann, and U. Zastrau. Thomson scattering from near-solid density plasmas using soft X-ray free electron lasers. *High En. Dens. Phys.*, 3:120, 2007.

[159] R. R. Faeustlin, U. Zastrau, S. Toleikis, I. Uschmann, E. Foerster, and Th. Tschentscher. A compact soft X-ray spectrograph combining high efficiency and resolution. *J. Instrum.*, 5, 2010.

[160] E. Allaria, R. Appio, L. Badano, W. A. Barletta, S. Bassanese, S. G. Biedron, A. Borga, E. Busetto, D. Castronovo, P. Cinquegrana, S. Cleva, D. Cocco, M. Cornacchia, P. Craievich, I. Cudin, G. D'Auria, M. Dal Forno, M. B. Danailov, R. De Monte, G. De Ninno, P. Delgiusto, A. Demidovich, S. Di Mitri, B. Diviacco, A. Fabris, R. Fabris, W. Fawley, M. Ferianis, E. Ferrari, S. Ferry, L. Froehlich, P. Furlan, G. Gaio, F. Gelmetti, L. Giannessi, M. Giannini, R. Gobessi, R. Ivanov, E. Karantzoulis, M. Lonza, A. Lutman, B. Mahieu, M. Milloch, S. V. Milton, M. Musardo, I. Nikolov, S. Noe, F. Parmigiani, G. Penco, M. Petronio, L. Pivetta, M. Predonzani, F. Rossi, L. Rumiz, A. Salom, C. Scafuri, C. Serpico, P. Sigalotti, S. Spampinati, C. Spezzani, M. Svandrlik, C. Svetina, S. Tazzari, M. Trovo, R. Umer, A. Vascotto, M. Veronese, R. Visintini, M. Zaccaria, D. Zangrando, and M. Zangrando. Highly coherent and stable pulses from the FERMI seeded free-electron laser in the extreme ultraviolet. *Nat. Photonics*, 6:699–704, 2012.

[161] W. F. Schlotter, F. Sorgenfrei, T. Beeck, M. Beye, S. Gieschen, H. Meyer, M. Nagasono, A. Föhlisch, and W. Wurth. Longitudinal coherence measurements of an extreme-ultraviolet free-electron laser. *Opt. Lett.*, 35:372–374, 2010.

[162] S. Roling, B. Siemer, M. Wöstmann, H. Zacharias, R. Mitzner, A. Singer, K. Tiedtke, and I. A. Vartanyants. Temporal and spatial coherence properties of free-electron-laser pulses in the extreme ultraviolet regime. *Phys. Rev. ST Accel. Beams*, 14:080701, 2011.

[163] R. Mitzner, B. Siemer, M. Neeb, T. Noll, F. Siewert, S. Roling, M. Rutkowski, A.A. Sorokin, M. Richter, P. Juranic, K. Tiedtke, J. Feldhaus, W. Eberhardt, and H. Zacharias. Spatio-temporal coherence of free electron laser pulses in the soft x-ray regime. *Opt. Express*, 16:19909–19919, 2008.

[164] Thomas Fennel, private communication.

[165] E. Springate, N. Hay, J.W.G. Tisch, M.B. Mason, M.H.R. Hutchinson T. Ditmire, and J.P. Marangos. Explosion of atomic clusters irradiated by high-intensity laser pulses: Scaling of ion energies with cluster and laser parameters. *Phys. Rev. A*, 61:063201, 2000.

[166] L. Schroedter, M. Müller, A. Kickermann, A. Przystawik, S. Toleikis, M. Adolph, L. Flückiger, T. Gorkhover, L. Nösel, M. Krikunova, T. Oelze, Y. Ovcharenko, D. Rupp, M. Sauppe, D. Wolter, S. Schorb, C. Bostedt, T. Möller, and T. Laarmann. Hidden charge states in soft-x-ray laser-produced nanoplasmas revealed by fluorescence spectroscopy. *Phys. Rev. Lett.*, 112:183401, May 2014.

[167] J.A. Bittencourt. *Fundamentals of plasma physics*. Springer, 3rd edition, 2004.

[168] J. Zweiback, T. Ditmire, and M. D. Perry. Femtosecond time-resolved studies of the dynamics of noble-gas cluster explosions. *Phys. Rev. A*, 59:R3166–9, 1999.

[169] T. Döppner, S. Teuber, M. Schumacher, J. Tiggesbäumker, and K.-H. Meiwes-Broer. Charging dynamics of metal clusters in intense laser fields. *Appl. Phys. B*, 71:357–360, 2000.

[170] T. Döppner, Th. Fennel, P. Radcliffe, J. Tiggesbäumker, and K.H. Meiwes-Broer. Strong field dual-pulse excitation of Ag_N: A charge selective analysis of the Coulomb Explosion. *Eur. Phys. J. D*, 36:165–171, 2005.

Acknowlegment

Curriculum Vitae

26 March 1989	born in Minsk, Soviet Union
1995 - 2002	School No. 74, Minsk
2002 - 2006	School No. 51, Minsk
2006	Bronze Medal at 37th International Physics Olympiad, Singapore
2006 - 2011	Belarusian State University, Physics faculty, Diplom with honor, Minsk
2011 - 2018	University Rostock, Institute of Physics, PhD - student, Rostock

Selbständigkeitserklärung

Hiermit versichere ich, dass ich die vorliegende Arbeit selbständig angefertigt und ohne fremde Hilfe verfasst habe, keine außer den von mir angegebenen Hilfsmitteln und Quellen dazu verwendet habe und die den benutzten Werken inhaltlich und wörtlich entnommenen Stellen als solche kenntlich gemacht habe.

Rostock, 24. August 2018

Dzmitry Komar